AGU PUBLICATIONS

JGR

Journal of Geophysical Research: Oceans

RESEARCH ARTICLE

10.1002/2016JC011774

Air-sea interaction at the Southern Brazilian Continental Shelf: In situ observations

L. P. Pezzi[1], R. B. Souza[2], P. C. Farias[2], O. Acevedo[3], and A. J. Miller[4]

[1]Earth Observation General Coordination, National Institute for Space Research-OBT/INPE, São José dos Campos-São, Paulo, Brazil, [2]Southern Regional Center for Space Research, National Institute for Space Research-CRS/INPE, Santa Maria-Rio Grande do Sul, Brazil, [3]Department of Physics, Federal University of Santa Maria-UFSM, Santa Maria-Rio Grande do Sul, Brazil, [4]Scripps Institution of Oceanography, University of California, San Diego, California, USA

Key Points:
- The strong cross-shelf thermal gradients of the southern Brazilian Continental shelf are a key seasonal feature in the area
- The gradients and the presence of the La Plata Plume waters are known to affect the biology of the area
- The effects of these gradients on the local marine atmospheric boundary layer and the air-sea fluxes of heat are first investigated here using in situ observations.

Correspondence to:
L. P. Pezzi,
luciano.pezzi@inpe.br

Citation:
Pezzi, L. P., R. B. Souza, P. C. Farias, O. Acevedo, and A. J. Miller (2016), Air-sea interaction at the Southern Brazilian Continental Shelf: In situ observations, *J. Geophys. Res. Oceans*, *121*, 6671–6695, doi:10.1002/2016JC011774.

Received 11 MAR 2016
Accepted 12 AUG 2016
Accepted article online 18 AUG 2016
Published online 10 SEP 2016

Abstract The influence of the cross-shelf oceanographic front occurring between the Brazil Current (BC) and the Brazilian Coastal Current (BCC) on the local Marine Atmospheric Boundary Layer (MABL) is investigated here. This front is typical of wintertime in the Southern Brazilian Continental Shelf (SBCS) and this is the first time that its effects are investigated over the above MABL. Here we analyze variability, vertical structure, and stability of MABL as well as heat fluxes at air-sea interface, across five oceanographic transects in the SBCS made during a winter 2012 cruise. Local thermal gradients associated with mixing between distinct water masses, play an essential role on MABL modulation and stability. Although weaker when compared with other frontal regions, the cross-shelf thermal gradients reproduce exactly what is expected for open ocean regions: Stronger (weaker) winds, lower (higher) sea level pressure, and a more unstable (stable) MABL are found over the warm (cold) side of the oceanographic front between the BC (warm) and coastal (cold) waters. Our findings strongly support the coexistence of both known MABL modulation mechanisms: the static and hydrostatic MABL stability. This is the first time that these modulation mechanisms are documented for this region. Turbulent fluxes were found to be markedly dependent on the cross-shelf SST gradients resulting in differences of up to 100 $W.m^{-2}$ especially in the southernmost region where the gradients were more intense.

1. Introduction

The Southern Brazilian Continental Shelf (SBCS) and adjacent areas are undertaking intense scrutiny within the scientific literature since the 1990 decade for its important role on several issues including fisheries [*Haimovici*, 1997; *Matsuura*, 1998; *Sunye and Servain*, 1998; *Cergole et al*., 2002; *Legey and Jablonski*, 2004; *Gigliotti et al*., 2010; *Soares et al*., 2011; *Dias et al*., 2014, *D'agostine et al*., 2015], phytoplankton ecology [*Ciotti et al*., 1995; *Brandini et al*., 2007, 2014; *Palóczy et al*., 2014], and physical processes [*Piola and Rivas*, 1997; *Guerrero and Piola*, 2008; *Lentini et al*., 2000; *Piola et al*., 2000; *Souza and Robinson*, 2004; *Palma et al*., 2008; *Möller et al*., 2008; *Matano et al*., 2014; *Guerrero et al*., 2014] among others.

Möller et al. [2008] describe that the meteorological conditions of fall to winter seasons in the South Atlantic Ocean are responsible for the development and progression of a coastal current that flows northeastern ward confined to the coast of Uruguay and the SBCS. Together with a predominance of winds in fall and winter from the southwest, the increase of precipitation in these seasons causes an increment on the La Plata river discharge. The La Plata flow, when reaching the outskirts of the river's mouth, tends to be drifted toward the north into the Uruguayan coast and the SBCS by the prevailing winds and geostrophic balance [*Piola et al*., 2008; *Möller et al*., 2008]. The current transporting these waters is known by the names of Brazilian Coastal Current (BCC) [*Souza and Robinson*, 2004] or Rio Grande Current [*Zavialov et al*., 2002] and is considered a seasonal current occurring over the SBCS during wintertime. The current typically carries the coastal waters originated from the La Plata river and, owing to the characteristics of its spreading over the shelf, these waters were baptized as the La Plata Plume (LPP) [*Piola et al*., 2000, 2008; *Möller et al*., 2008]. The BCC carries cold, low salinity waters and flows opposite to the BC that carries warm and salty waters at the shelf break and open ocean regions [*Peterson and Stramma*, 1991]. The sheering between BC and BCC along the shelf break region promotes intense across-shore thermal, surface (SST), and subsurface

gradients as well as mixing between the coastal, La Plata Plume Water (PPW), and Tropical Water (TW) along its path.

Acknowledging the very complex oceanographic processes occurring in the SBCS (recently reported by *Matano et al*. [2014] and *Guerrero et al*. [2014]), we shall remember that the meteorological conditions of the area, especially in wintertime, are no fewer complexes. The adjacent regions of the Southwestern Atlantic Ocean and the southern region of South America are regions of high frequency of cyclogenesis. In the early 1990s, *Gan and Rao* [1991] described two centers of maximum cyclogenesis occurrence over Uruguay and at the Gulf of San Matias in the Argentinean Patagonia. More recently, *Hoskins and Hodges* [2005] described the importance of the cyclogenesis and the Storm Tracks of the Southern Hemisphere and their importance for the weather and climate. Using new data in relation to *Gan and Rao* [1991], the authors summarized in their Figure 6 the trajectories of all cyclonic systems that they identified as originated in the cyclogenetic region near 30°S over South America, a region that matches exactly with the location of the SBCS. Cyclones can travel around the Southern Hemisphere along the South Atlantic toward the Indian Ocean and the Pacific although track density data show that they are more frequent close to the South American continent. Statistics for cyclogenesis made by *Hoskins and Hodges* [2005] corroborated the ones found by *Gan and Rao* [1991]. The availability of more recent, global data used by *Hoskins and Hodges* [2005] resulted in the addition of another cyclogenesis region located at the tip of the Antarctic Peninsula south of the Atlantic Ocean.

The mechanisms of cyclones formation at Southeast of South America are attributed to a conjunction of factors. Among them, during the winter is the baroclinic instability because of the strong frontal thermal gradient, which is associated to the conversion of potential energy into kinetic energy of the disturbance, intensifying the secondary circulations and rotational motions of the cyclone that will increase the western (high levels) wind shear [*Gan and Rao*, 1991]. While in the summer the cyclogenesis systems will rely on hydrodynamic instability.

Innocentini and Caetano Neto [1996], *Seluchi and Saulo* [1998], and *Piva et al*. [2008, 2011] are among the authors that reported cyclogenetic events in the coast of Brazil describing the associated intense winds and rain. *Piva et al*. [2011] describe that warm waters will contribute to generation of intense latent and sensible heat fluxes at surface, which in turns favor the cyclone intensification. The formation of extratropical cyclones occurs in a baroclinic environment, and the latent and sensible heat released by the warm waters affect only their intensity, contrasting to what happens in tropical cyclones, where the latent and sensible heat fluxes play an essential role to their genesis and development [*Davis and Bosart*, 2004]. Another important factor, although barely studied in this area of the world, is the influence of the ocean-continent thermal contrasts. Once cyclogenesis often occurs near to the coast, it is expected to be highly influenced by the sea surface thermodynamics conditions. Thus observing Southwest South Atlantic and knowing these exchanges processes between the ocean and atmosphere are determinants.

The first documented hurricane happening in the South Atlantic occurred in March 2004 when an extratropical cyclone evolved to become Hurricane Catarina (reaching category 1). Its diagnosis and life cycle was quite complex, as argued by *McTaggart-Cowan et al*. [2006]. Among this diagnostics, it has been established that one of its causes was the displacement of the hurricane toward relatively warmer waters that were present along its track [*Davis and Bosart*, 2004; *McTaggart-Cowan et al*., 2006; *Vianna et al*., 2010]. The hurricane crossed the SBCS reaching the coast of southern Brazil at the latitude of 29°S. Air-sea interaction processes had a key role in this system, as Hurricane Catarina interacted strongly with four warm core oceanic eddies [*Vianna et al*., 2010]. From these authors' analysis, it is possible to infer that the MABL stability played a fundamental role since the SST was considerably high (24°C) over the warm eddies than the surface air temperature (14°C). This is an ideal condition to turn into MABL unstable as shown by *Pezzi et al*. [2005, 2009] over the BMC region in the South Atlantic.

Cold fronts are very frequent during winter in southern Brazil. The process of cold front formation is dependent on the meridional gradient of air temperature that is more intense during winter due to the approximation of polar air masses [*Lupo et al*., 2001]. *Andrade et al*. [2005] analyzed the cold fronts passage in South America during the period from 1980 to 2002 and demonstrated that the frequency of passages rises with the latitude. The authors also described that the displacements of the synoptic atmospheric system in the latitudinal band of 25°S–30°S are more frequent at the coastal zones than over the South American

continent. *Fedorova* [1999] reports that ahead of a cold front passage in the region that comprehends the SBCS the winds shit from (coming from) the north and both the air temperature and humidity increase. During the cold front passage, together with precipitation, the atmospheric pressure decreases to a minimum and the air is saturated or close to saturation. After the passage, the atmospheric conditions change again with instabilities being replaced by the entrance of a postfrontal (dry, cold) air mass. In this situation, there is a gradual reduction of the cloudiness and a dominance of winds coming from the south.

Early studies investigating ocean-atmosphere interactions over regions of strong thermal gradients in the ocean [*Lindzen and Nigam*, 1987; *Hayes et al*., 1989; *Wallace et al*., 1989] emphasized the influence of the SST on the surface winds and the MABL structure and stability modulation. These studies made over the eastern Equatorial Pacific Ocean suggested two distinct mechanisms for the ocean-atmosphere interaction. The hypothesis of *Lindzen and Nigam* [1987] attributes the surface wind modulations to the hydrostatic stability, as a consequence of the variations of the Sea Level Pressure (SLP). Lower (high) pressures would be found over warmer (cooler) waters and, as a consequence, stronger winds would be found where the highest pressure or SST gradients are located. *Wallace et al*. [1989] on the other hand proposed that positive SST anomalies induce changes on the MABL static stability. In this case, air buoyancy and turbulence intensity would increase over warmer waters, thus reducing the MABL vertical wind shear, and generating stronger winds at the sea surface. An opposite situation would be expected over colder waters.

The above mentioned mechanisms were investigated in the extra tropical region of the BMC in the South Atlantic Ocean by *Tokinaga et al*. [2005], *Pezzi et al*. [2005, 2009], *Acevedo et al*. [2010], and *Camargo et al*. [2013]. The last authors used in situ and numerical modeling data to suggest the coexistence of both *Lindzen and Nigam* [1987] and *Wallace et al*. [1989] mechanisms to sustain the MABL stability. Also, some studies have argued that midlatitude SST effects in oceanographic fronts may extend from the MABL into the upper atmosphere [*Minobe et al*., 2008; *Kilpatrick et al*., 2015].

The motivation of present study lies on the fact that BC/BCC front (often known as the Subtropical Shelf Front (STSF) when the proper water masses are found) [see *Piola et al*., 2000, 2008; *Möller et al*., 2008], although a typical coastal front [*Souza and Robinson*, 2004], presents across-shore SST gradients similar to the ones found in other frontal regions of the World Ocean such as the BMC, the Gulf Stream, and the Kuroshio Current. Our major objective is to describe if and how the local thermal gradients associated with the mixing between distinct water masses in the SBSB region during winter modulate the MABL and its stability across the study region. For achieving our objective, we used in situ oceanographic and meteorological data taken during a research cruise performed between 12 and 20 June 2012 (Austral winter).

In addition, we analyzed both parameterized and directly measured heat fluxes (Figure 1) in the region and period of this study using surface data collected through traditional methods and by applying the Eddy Covariance (EC) technique to data collected by instruments mounted on a micrometeorological tower installed onboard. As well as describing the sensible and latent fluxes between the ocean and the atmosphere across the BC/BCC front. We also compared EC estimations with bulk parameterizations and reanalysis data with the objective of

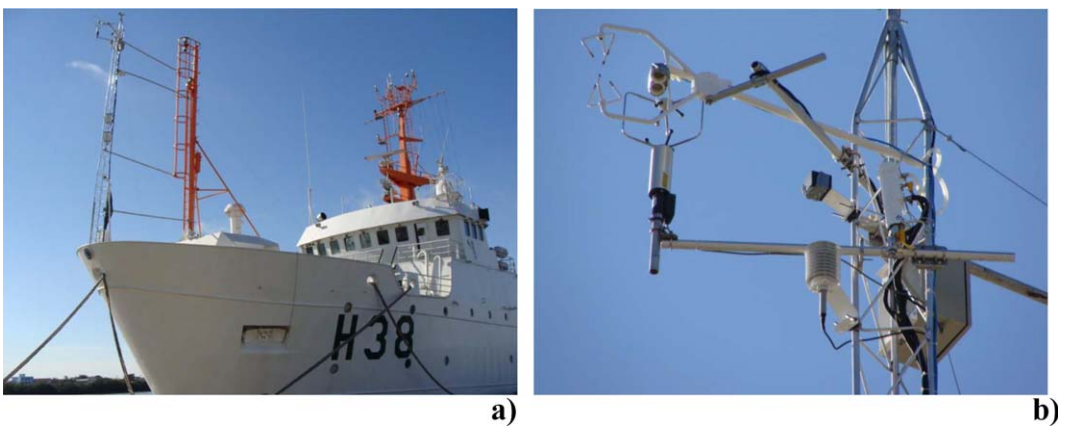

Figure 1. Details of *RV Cruzeiro do Sul* and her micrometeorological tower. Anemometers, motion sensor, GPS, and gas inlets were mounted at approximately 14 m above the ocean surface. Gas analyzers were located in the Bosun's locker, directly below the ship bow's mast.

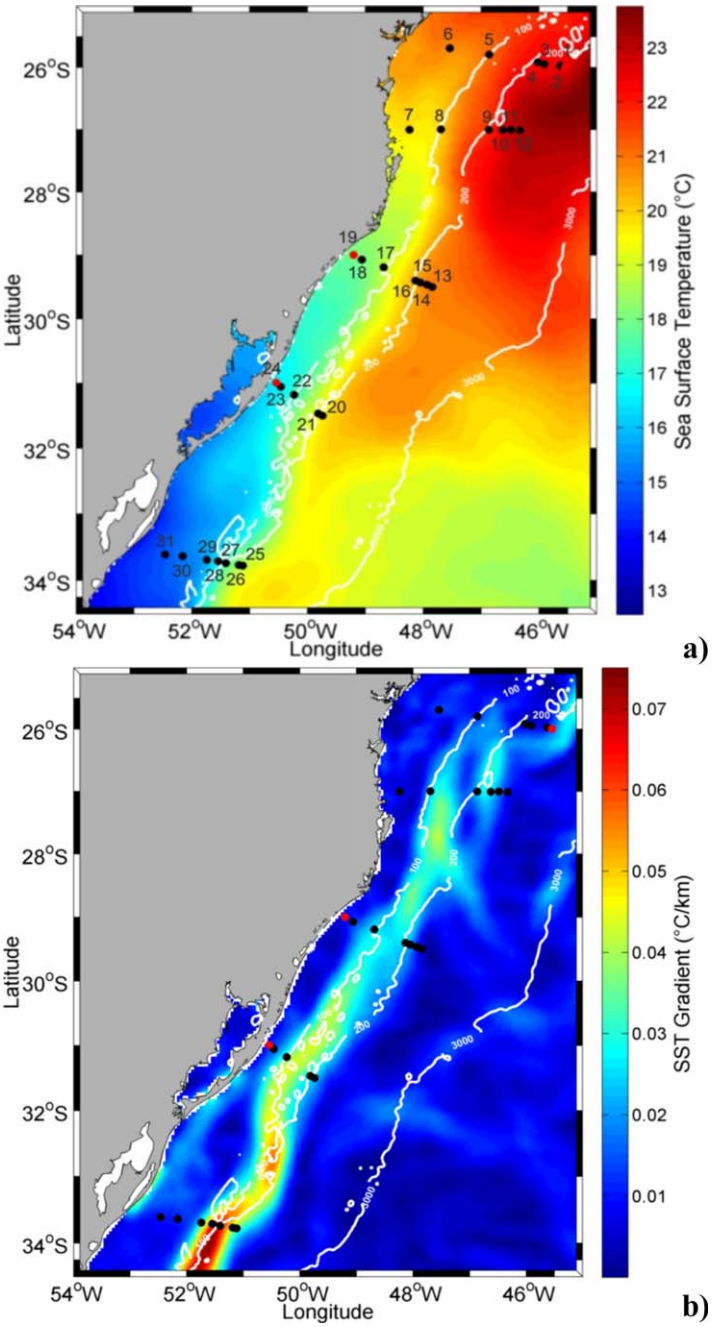

Figure 2. (a) Satellite SST monthly averaged map of June 2012 and the oceanographic stations made along the five across-shore transects during the ACEx/SIMTECO cruise. (b) SST zonal gradients present in the region along the BC/BCC front during June 2012.

estimating possible biases in the measurements. This is an important issue that can help to improve the quality of numerical weather forecast, in the future.

In order to support our conclusions, besides describing the surface oceanographic conditions of the SBCS during the time of the research cruise, we also performed an analysis of the prevailing meteorological synoptic conditions at that time. Physical oceanography and CO_2 fluxes data were also collected during the cruise. The analysis of this data is still underway and will soon appear in the literature. This paper is organized as follows: section 2 presents the study region and the data and methodology used here. Section 3 presents the meteorological synoptic analysis made for the period of this study. The vertical structure of the MABL and its stability mechanisms are presented in section 4. The last section includes our concluding remarks.

2. Material and Methods

Our present lack of knowledge on the governing processes of the ocean-atmosphere interaction in the Southwestern Atlantic Ocean and the relation between physical processes, especially the MABL stability and heat fluxes with the CO_2 fluxes in this region motivated the establishment of an innovative research project named *Atlantic Carbon and Fluxes Experiment* (ACEx). ACEx was a Brazilian funded project aimed to boost our knowledge on physical and chemical ocean-atmosphere exchanges in the Southwestern Atlantic Ocean by both collecting new in situ data using research vessels and by implementing a ocean-atmosphere, eddy resolving coupled model apt to cope with the impacts of the local ocean mesoscale variability on the MABL thermodynamics. However, this paper is focused on the results that arose from in situ data.

Project SIMTECO (*Monitoring System for the Weather, Climate and Ocean in Southern Brazil*) was set in complement to ACEx aiming to study the meteorological and oceanographic processes that affect the weather and the climate of the southern region of Brazil. During the period between 12 and 20 June 2012, ACEx and SIMTECO

Table 1. Descriptions of the ACEx/SIMTECO Cruise[a]

T	N°/Front Side	Latitude (°S)	Longitude (°W)	Date and Local Time	MABL Top Height (m)	Mean Atmospheric Synoptic Condition	T_{air} (°C)	SST (°C)
1	02-W	25.97	45.63	12 June 13:10h	880	Light to moderated winds	21.9	22.5
	03-W	25.95	45.90	12 June 15:40h	700	and predominance South	21.9	22.3
	04-W	25.91	46.02	12 June 18:10h	690	Atlantic High Pressure	21.0	22.0
	05-C	25.79	46.86	13 June 00:20h	1010	System	20.6	21.1
	06-C	25.68	47.54	13 June 06:45h	1300		20.4	20.8
2	07-C	27.00	48.24	13 June 17:25h	1110	Predominance of South	19.9	20.2
	08-C	27.00	47.69	13 June 22:05h	500	Atlantic High Pressure	19.6	19.4
	09-W	27.01	46.86	14 June 08:20h	1450	System	21.7	21.4
	10-W	27.03	46.62	14 June 11:50h	1310		23.8	23.2
	11-W	27.01	46.48	14 June 13:50h	1330		22.6	23.0
	12-W	27.02	46.32	14 June 16:00h	1390		22.6	23.8
3	13-W	29.51	47.84	15 June 11:05h	770	Extra tropical cyclone off	21.2	21.4
	14-W	29.50	47.92	15 June 12:50h	970	shore at 40°S and 34°W	21.1	21.7
	15-W	29.43	48.05	16 June 11:20h	250	winds blowing from	21.2	22.0
	16-W	29.40	48.14	16 June 13:30h	320	south, causing an	19.7	20.9
	17-C	29.19	48.68	16 June 18:35h	390	accentuated cold	17.9	18.3
	18-C	29.06	49.05	16 June 22:40h	1200	advection	16.6	18.8
4	20-W	31.52	49.77	17 June 21:55h	600	Extra-tropical cyclone south-	18.4	19.9
	21-W	31.48	49.84	18 June 01:20h	800	east of the study region	16.9	19.4
	22-C	31.18	50.24	18 June 05:30h	590		17.6	16.8
	23-C	31.06	50.46	18 June 08:00h	670		16.8	17.0
5	25-W	33.75	51.12	19 June 09:45h	1040	Incursion of post-frontal air	14.2	18.5
	26-W	33.77	51.19	19 June 12:55h	1180	mass. Intense cold	13.9	17.0
	27-W	33.74	51.44	19 June 15:20h	920	advection in the region	13.0	19.5
	28-W	33.71	51.55	19 June 17:30h	830		12.6	17.0
	29-C	33.69	51.75	19 June 19:15h	820		12.4	14.8
	30-C	33.63	52.16	19 June 22:40h	660		11.2	14.7
	31-C	33.60	52.45	20 June 01:45h	580		11.5	14.4

[a]Columns indicate (1) the across-shore transects taken during the cruise; (2) the transect number and position in the BC/BCC front: warm (W) or cold (C) front side; (3,4,5) location and time where the sampling were made; (6,7) MABL top height and mean atmospheric synoptic condition; and (8,9) air and sea surface temperatures.

performed a joint oceanographic cruise onboard the Brazilian Navy Research Vessel (*RV*) *Cruzeiro do Sul* (Figure 1). The period and region covered by the ACEx/SIMTECO cruise were planned to sample in time and space most of the across-shore processes typical of the BC/BCC front including the strong SST, salinity, and chlorophyll gradients between the coastal and the offshore water masses carried by the BC and BCC.

2.1. Study Region and Sampling Stations

The study region covered by the ACEx/SIMTECO cruise is located in the SBCS comprising the coastal region and part of the continental shelf break with depths between 500 and 600 m, as shown in Figure 2. The sampling stations were performed along five cross-shore transects located between the cities of Paranaguá (Paraná State, Brazil—25.8°S) and Chuí (Rio Grande do Sul State, Brazil—33.7°S). The transects were aimed to cross the BC/BCC SST gradients and were performed from north to south being named as (i) T1-Paranaguá; (ii) T2-Itajai; (iii) T3-Araranguá; (iv) T4-Mostardas; and (v) T5-Chuí (Figure 1). Along the five transects, a total of 31 oceanographic stations were taken (Table 1). Simultaneous launchings of atmospheric radiosondes from the ship were made. Complementary meteorological data along the entire route of the *RV Cruzeiro do Sul* were obtained by the onboard AWS and by a micrometeorological tower installed at the ship's bowl.

2.2. SST and Meteorological Analysis

Satellite SST images were analyzed previously to and during the ACEx/SIMTECO cruise aiming to identify regions of strong SST gradients and plan the cruise track. The 18.5°C isotherm was used mark the oceanographic front between BC and BCC [*Souza and Robinson*, 2004]. Satellite SST data were obtained from the *Operational Sea Surface Temperature and Sea Ice Analysis* (OSTIA), a blended product using satellite data from infrared, visible, and radiometer sensors as well as in situ data from drifting and moored buoys. Owing to the cloud coverage of the region during the cruise, a mean SST composite made with SST maps for the period 12–20 June 2012 was also generated. This mean image was used to characterize the spatial variability of the SST during the cruise and also to produce a map of the SST gradients in the region. However here we present SST mean field for the whole month of June 2012 (Figure 2). More information about this data

set can be found in *Stark et al*. [2007]. OSTIA data can be accessed from http://podaac.jpl.nasa.gov/dataset/UKMO-L4HRfnd-GLOB-OSTIA.

Gridded analysis data (*Climate Forecast System version 2*-CFSv2) from the National Center for Environmental Prediction (NCEP) at 0.5° grid spacing were used for assessing the atmospheric synoptic conditions during the ACEx/SIMTECO cruise. This data set was used together with NCEP 2 reanalysis version 2 to compare the EC heat fluxes measurements. More information about this data set can be found in *Saha et al*. [2010, 2014] and *Kalnay et al*. [1996]. CFSv2 data can be accessed in http://rda.ucar.edu/datasets/ds094.0/. Sea level pressure charts produced by the Directory of Hydrography and Navigation (DHN) from Brazilian Navy (MB) were used to analyze the main synoptic systems acting during the cruise period. These charts can be download from DHN website https://www.mar.mil.br/dhn/chm/meteo/prev/cartas/cartas.htm. Several infrared images from the GOES-12 Imager per day were obtained from the *Brazilian Center for Weather Forecast and Climate Studies* (CPTEC/INPE) and used to complement the synoptic analysis made here in section 3.1. These images can be accessed in http://satelite.cptec.inpe.br/acervo/goes.formulario.logic. In order to complement our synoptic analysis, surface wind data from the ship's *Automatic Weather Station* (AWS, better described later on this text) are also used.

2.3. Traditional In Situ Measurements and Heat Flux Parameterizations

The oceanographic data used in this paper refer only to the SST and temperature profiles taken by *Expandable Bathy-Thermographs* (XBTs). High-frequency SST and surface salinity data were collected by a SeaBird Electronics thermosalinographer installed onboard *RV Cruzeiro do Sul*. The use of radiosonde, XBT, and thermosalinographer data in order to allow a complete description of the MABL and its modulation by oceanographic fronts in the Southwestern Atlantic Ocean has been proved useful by *Pezzi et al*. [2005, 2009]. The other traditional oceanographic measurements taken during the ACEx/SIMTECO cruise at each oceanographic station by *Conductivity, Temperature, Depth* (CTD) casts. During the cruise chlorophyll-a and phytoplankton measurements were also measured.

Physical parameters of the atmosphere inside the MABL were measured using atmospheric radiosondes (Vaisala model RS90) launched from the vessel's rear deck. Primary parameters measured include the atmospheric pressure, the air temperature, and the relative humidity (RH) at 0.5 Hz frequencies along the rising of the radiosondes in the atmosphere. The position of the radiosonde balloons was traced with a Global Position System (GPS) device onboard the ship and used to estimate the wind speed and direction. The vertical resolution of the radiosondes' sampling was between 7 and 10 m in the first kilometer of the MABL. Other atmospheric variables were automatically derived by the radiosonde receptor in real time: potential temperature (θ_{air}), dew point temperature (T_d), ascension rate, geopotential height, and mixing ratio or specific humidity (q). The MABL sampling positions are indicated in Figure 1 by the black circles.

As quoted before, *RV Cruzeiro do Sul* has an AWS allowing her to take underway meteorological measurements. The sensors were mounted above the ship's bridge at approximately 15 m above the sea surface. Observed meteorological parameters include the air temperature, the wind speed and direction, and the sea level atmospheric pressure. In order to estimate the ocean-atmosphere sensible and latent heat fluxes from these observed meteorological parameters, we used the well-known, bulk parameterization proposed by *Fairall et al*. [1996]. SST data for these parameterizations were taken from the ship's thermosalinographer. The basis of the parameterization algorithm applied here lies on the Monin-Obukhov similarity theory that considers the flux as constant at the sea surface layer. Although *Fairall et al*. [1996] has developed their bulk formulae for the Tropical Ocean, authors such as *Pezzi et al*. [2005, 2009] and *Acevedo et al*. [2010] had successfully used it for the BMC region in the Southwestern Atlantic Ocean.

2.4. Micrometerological Tower and Eddy Covariance Fluxes

As a technological development of project ACEx, a micrometeorological tower was adapted and installed at the bow of *RV Cruzeiro do Sul* (Figure 1). Attached sensors were used to make measurements of the ocean-atmosphere turbulent fluxes of momentum, heat, moisture, and CO_2 using the EC technique. The CO_2 fluxes measurements made during this cruise will be presented in separated article. EC returns direct measurements of the turbulent fluxes over an area with dimensions of 10^2-10^3 m^2. For computing the fluxes, high-frequency (20 Hz) wind measurements were made using a pair of three dimensional (3-D) sonic anemometers model CSAT3, Campbell Scientific. For performing corrections on the wind's 3-D components for

the ship's movements, a 3-axis inertial navigation system (MotionPak 2, Systrom Donner) measured linear accelerations and angular rates simultaneously to the wind measurements. A magnetic compass (model KVH C100) measured the ship's heading. The water vapor concentration in the atmosphere was measured using a fast-response, open-path infrared gas analyzer (IRGA) model LiCor LI7500. CO_2 concentration and an additional water vapor concentration in the atmosphere were measured using an enclosed IRGA model LiCor LI-7200. The anemometer, the motion sensor, the gas inlets for CO_2, and water vapor and a complementary GPS receptor were mounted in a tower fixed to the bow mast of the ship at approximately 14 m above the ocean's surface. The gas analyzers were located in the Bosun's locker, directly below the ship's bow mast. A complete and detailed description of the instruments including a diagram of their disposition in the tower is shown in *Farias* [2014].

The technique of correction for the movement used in this study was implemented by *Martins* [2015] who used the method proposed by *Miller et al*. [2010] to correct for the vertical component of the wind then reducing the uncertainties of the turbulent flux measurements affecting the accuracy of the EC estimates. The correction for the vertical component of the wind, *Martins* [2015] considers the real wind velocity as a sum of the apparent velocity (measured by the sonic anemometer) with the velocity of the sensor's movement in the same system of coordinates. Additional measurements for assessing the sensor's velocity include the rotational and translational velocities of the sensor as well as the ship's velocity. The rotational and translational velocities of the sonic anemometer are computed from measuring the accelerations and angular velocities with the inertial navigation system.

The turbulent fluxes of sensible heat (F_{SH}), latent heat (F_{LH}), and CO_2 (F_{CO2}) can be determined from the covariances between the fluctuations of vertical velocity and a respective scalar through the following expressions:

$$F_{LH} = \overline{\rho_a} c_p \overline{w'T'}, \tag{1}$$

$$F_{SH} = \overline{\rho_a} L_v \overline{w'q'} \tag{2}$$

$$F_{CO_2} = \overline{\rho_a} \overline{w'c'} \tag{3}$$

where, $\overline{\rho_a}$ is the density of dry air, c_p is the specific heat capacity of air, L_v is the latent heat of vaporization, q is specific humidity and w', T',r' and c' are the fluctuations of the vertical wind speed component, temperature, and mixing ratio of the water density vapor (H_2O) and CO_2 with dry air density $\left(r = \frac{\rho_{H_2O}}{\rho_a} \text{ and } c = \frac{\rho_{CO_2}}{\rho_a}\right)$.

To our knowledge, the ACEx/SIMTECO cruise performed the first EC measurements of heat and CO_2 fluxes between the ocean and the atmosphere in the Southwestern Atlantic Ocean. Additional high-frequency meteorological measurements (not used here) were made from other instruments installed in the bow's tower. They include air temperature, atmospheric pressure, relative humidity, and incident and leaving radiation. We would like to stress the fact that the main focus of this paper is not to deeply address the accuracy of the EC measurements and we leave these matters for future work. Instead, we focus our discussions on a processes study and the relations between the fluxes and the SST gradients in our study area. The EC technique has been widely used in many other studies to estimate turbulent ocean-atmosphere fluxes e.g., *McGillis et al*. [2001], *Pedreros et al*. [2003], *Miller et al*. [2004, 2008], *Huebert et al*. [2004], *Blomquist et al*. [2010], *Smith et al*. [2010], *Landwehr et al*. [2015], and *Flügge et al*. [2016]. Nonetheless, the improvement of ocean-atmosphere flux measurements' quality as well the addition of new areas being covered in the Global Ocean is object of current international effort.

3. Results

3.1. SST Fields and Synoptic Meteorological Analysis

Figure 2a presents the SST composite averaged for June 2012. The SST field reveals the presence of BC waters (mapped in colors ranging from yellow to red) in depths deeper than 200 m from the continental shelf break to the open ocean. BCC waters (in colors from blue to green) are found inside the continental shelf penetrating the SBCS. Isotherms between 18.5°C and 20°C can be used to map the center of the BC/BCC front [*Piola et al*., 2000; *Souza and Robinson*, 2004].

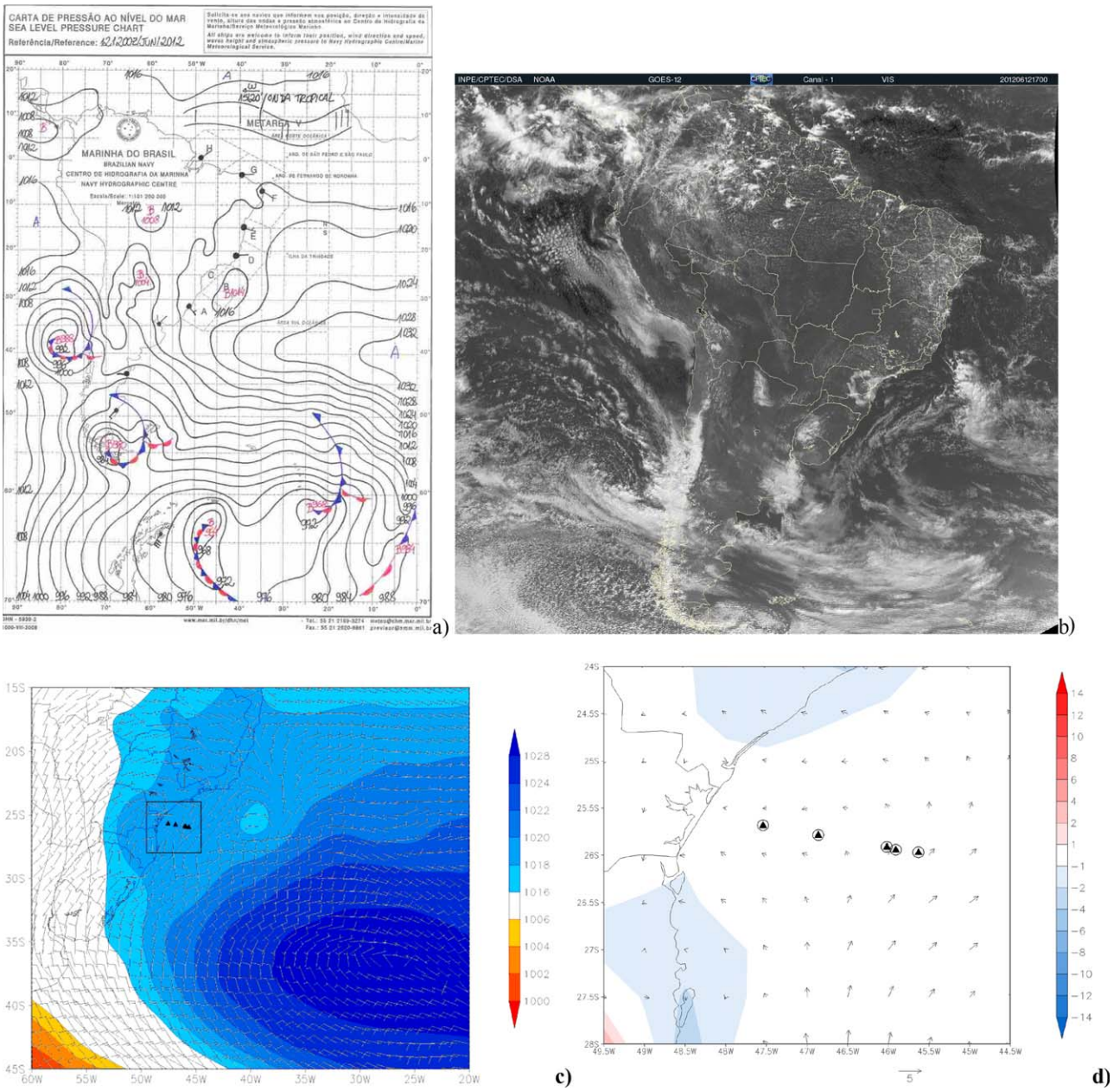

Figure 3. (top–bottom, left) Sea level pressure charts produced by the DHN from Brazilian Navy. (top–bottom, right) GOES-12 satellite image from the visible channel. (top to bottom, left) Sea level pressure (hPa) with superimposed wind at 1000 hPa (m.s^{-1}) from T1 to T5. (top–bottom, right) Thermal advection (°C.d^{-1}) with superimposed wind at 1000 hPa (m.s^{-1}) from T1 to. Black triangles denote sampling positions in each transect. The synoptic charts can be assessed in https://www.mar.mil.br/dhn/chm/meteo/prev/cartas/cartas.htm. Satellite images were downloaded from CPTEC/INPE in http://satelite.cptec.inpe.br/acervo/goes.formulario.logic.

Many physical MABL properties such as stability, surface wind stress, and air-sea fluxes exchanges are modified by the SST gradient associated by oceanic fronts and features (eddies) as already showed in the literature [*Xie*, 2004; *Chelton et al*., 2004; *Seo et al*., 2007; *Small et al*., 2008; *Pezzi et al*., 2009; *Acevedo et al*. 2010] and will be further discussed in this study. Because of that, we analyze here the map of the SST gradients found in the study region in Figure 2b. The maximum across-shelf SST gradients are coincident with the position of the BC/BCC front over the continental shelf break. In the southernmost part of our study area where the thermal gradients can reach 0.075°C.km^{-1} while in the northernmost part of the area they are about 0. 045°C.km^{-1}. This is due to the fact that the BCC is a seasonal current that progresses over the SBCS with maximum extension occurring only in August [*Souza and Robinson*, 2004]. Owing to the small presence of the Subantarctic Shelf Water in the region and period, a key water mass for the existence of the

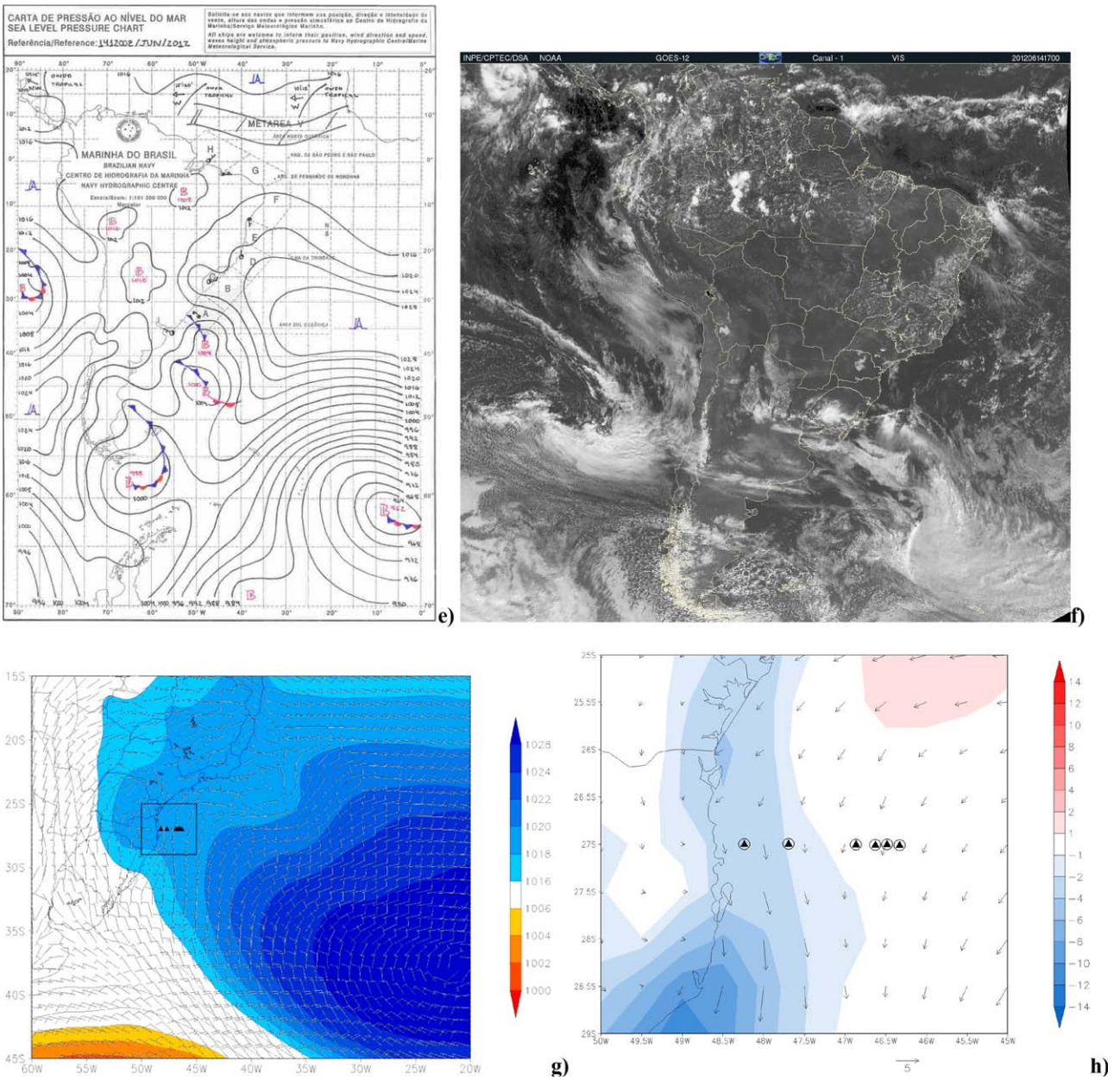

Figure 3. (continued)

Subtropical Shelf Front as defined by *Piola et al*. [2000] and *Möller et al*. [2008], we adopt the name BC/BCC for describing the region of higher lateral thermal gradients along our study area.

Although the oceanographic conditions of the area presented in Figure 2 can be considered fairly constant during the 9 days when the ship was at sea (from 12 to 20 June 2012), the meteorological conditions changed considerably in the same period. The cruise was performed starting from the north and, during the traveling of the ship from transects T1 (Paranaguá, northernmost transect) to T5 (Chuí, southernmost transect), several specific synoptic conditions of the atmosphere occurred. The importance of the synoptic meteorological analysis lies in the fact that, although the SST gradients may impose a specific forcing to the local MABL stability (discussed in section 4) and turbulent fluxes of heat and CO_2 (section 5) when no large-scale disturbances in the atmosphere are present [*Pezzi et al*., 2005, 2009], this may not be the case when transient systems such as cold fronts or cyclones are present.

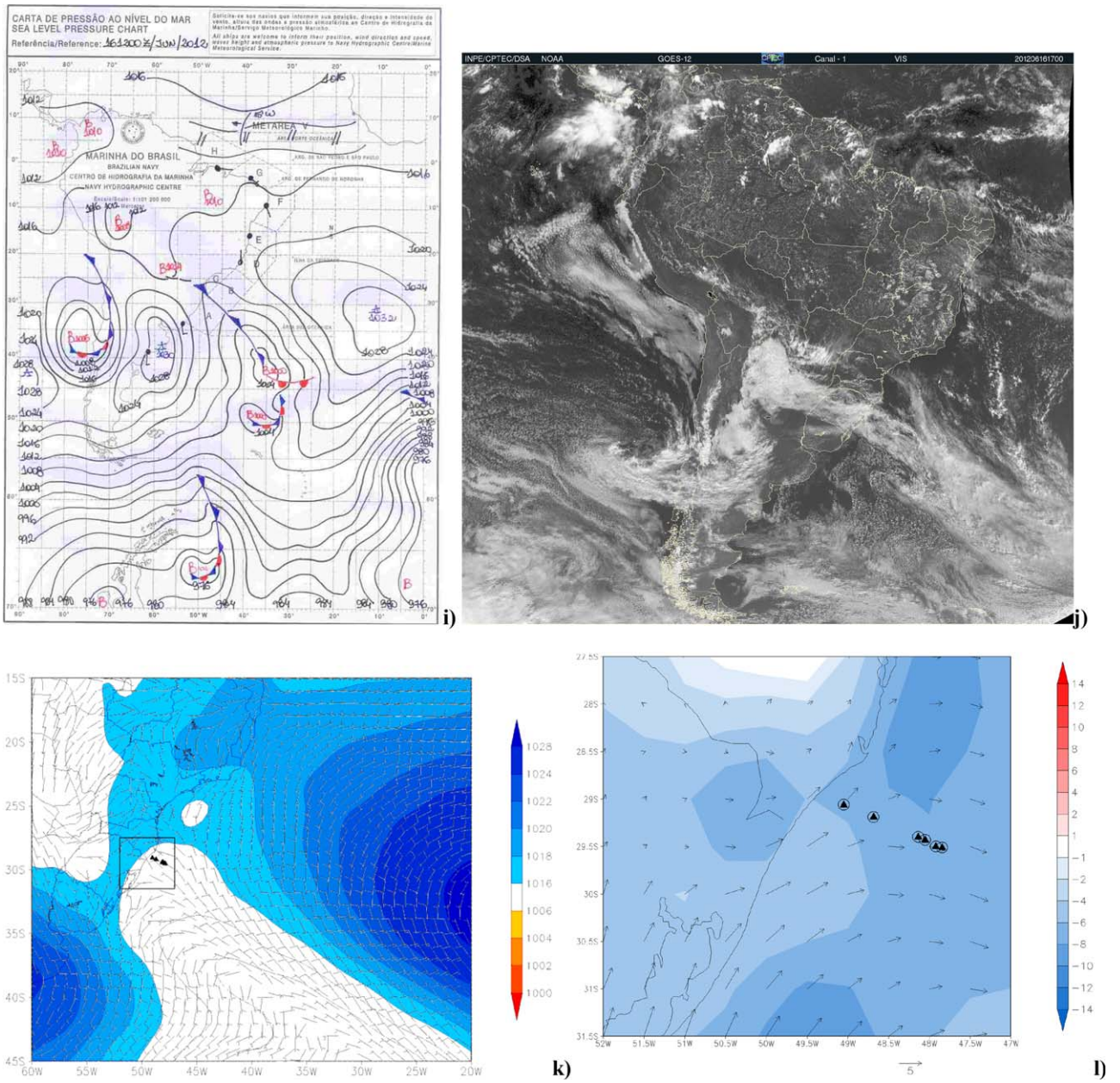

Figure 3. (continued)

Figure 3 presents the sea level pressure charts and satellite images that were used to diagnose the large-scale patterns of the synoptic conditions prevailing in the study area during the realization of the ACEx/SIMTECO cruise. The figure also displays a mesoscale view of the meteorological conditions (sea level pressure with superimposed surface winds) and a zoomed view of the surface winds and thermal advection averaged for the period of realization of each of the five sampling transects. To complement our synoptic analysis, surface wind data from the ship's AWS are shown in Figure 4.

In a general way, two very distinct weather conditions occurred during the whole cruise period: the typical predominance of the South Atlantic Subtropical High (SASH) of the South Atlantic Ocean followed by a cyclogenesis at the end of the cruise period. The SASH is a quasipermanent high pressure system that seasonally oscillates its center between higher (during Austral Summer) and lower (during the Austral winter) latitudes in the South Atlantic Ocean between a central annual mean position around 30°S and 25°W. This drives the winds in the western border of the South Atlantic Ocean to blow from the northern quadrant

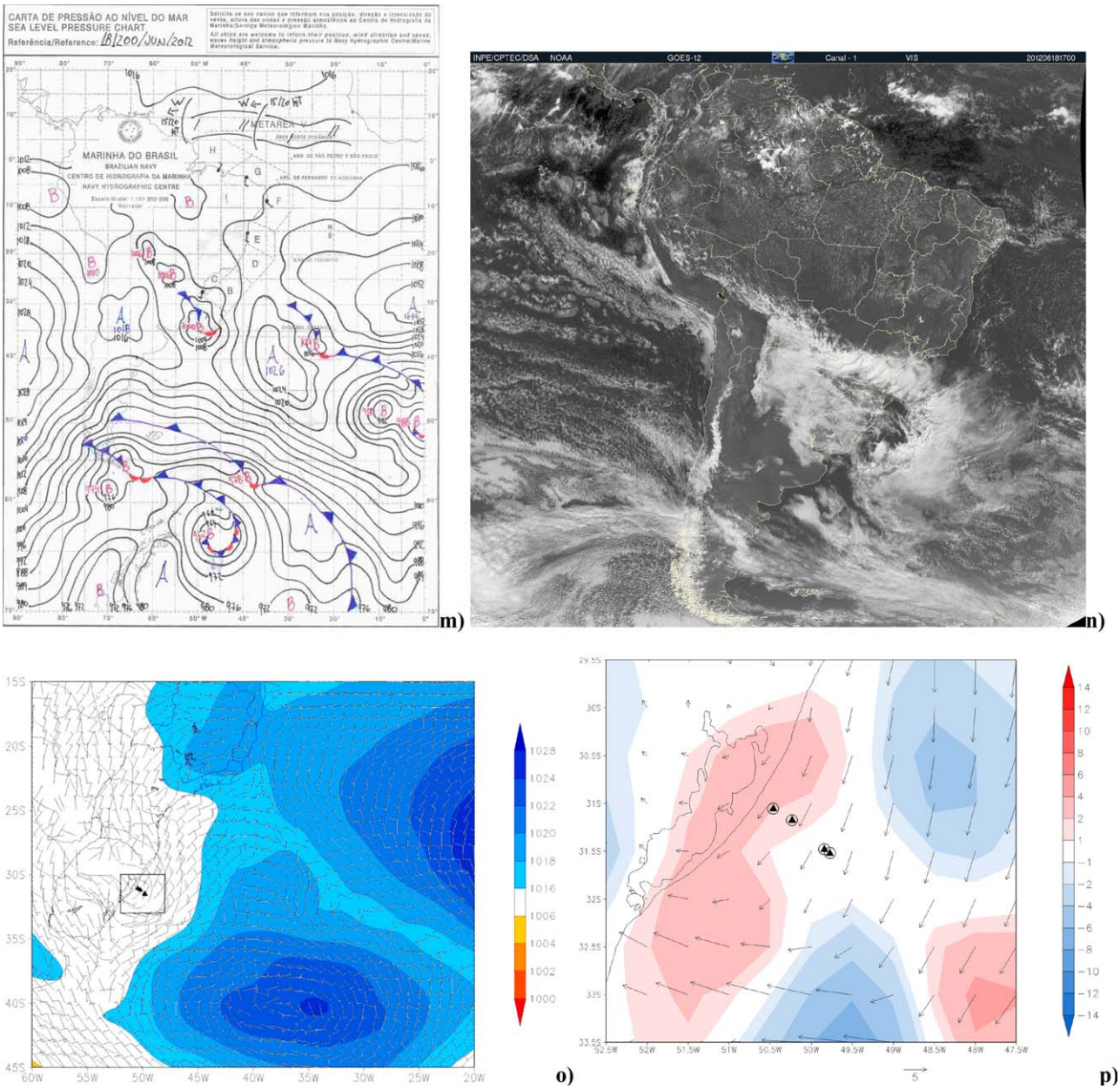

Figure 3. (continued)

when no frontal atmospheric system or cyclogenesis is present. Air temperatures in the SASH are high as a consequence of the intense solar radiation, characteristic of tropical latitudes where we have high humidity due to the intense evaporation of water from the sea [*Pezzi and Souza*, 2009].

Figures 3a–3d show that during T1 (held between 12 June 11:00h local time to 13 June 2012 06:45h local time from east to west) there were no frontal or transient atmospheric systems active over the study area. Instead, the ship was under the influence of a high pressure system. At the sea surface, wind conditions decreased from moderate ($\sim$6 m.s^{-1}) to light ($\sim$2 m.s^{-1}) winds in the course of the period with a strong shear and shift in direction over the BC/BCC front (Figure 4a). The synoptic analysis (Figures 3a and 3b) also indicated that no strong atmospheric pressure gradient was present. Further east to T1, it was possible to identify a cyclonic circulation in the lower troposphere (Figure 3c), favoring the intensity weakening of the SASH. During 12–13 June 2012, low warm clouds were observed at sea from visible (and infrared, not shown) GOES-12 images (Figure 3b). Figure 3c shows that even with a light wind

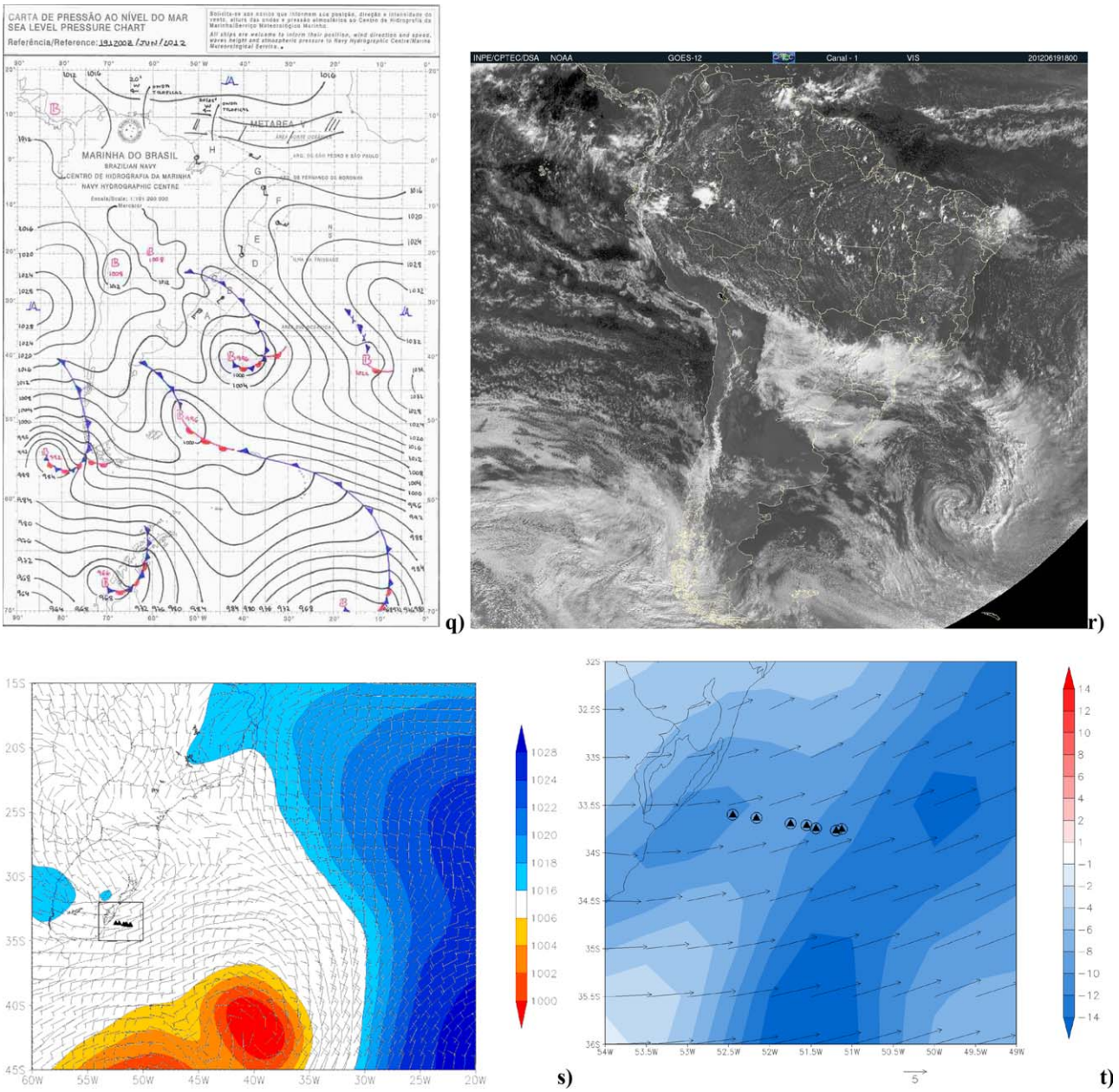

Figure 3. (continued)

blowing from the south towards the site of T1, there was an observed warm advection of up to 2°C.d^{-1} (Figure 3d).

When T2 was held (13 June 17:20h local time to 14 June 2012 15:10h local time from west to east), the large-scale synoptic condition was very similar to T1 with a prevailed SASH influence (Figures 3e–3h). Observations from the ship's AWS (Figure 4b) show the predominant wind direction from the north and northeast due to counter clockwise atmospheric circulation associated with the high-pressure system. Wind intensities fluctuated between ~4 and 9 m.s^{-1}. Even with winds blowing from the north due to SASH circulation (Figure 3e), a light cold thermal advection (expected when winds are from the south) is present in the sampling area (Figure 3h).

Pezzi and Souza [2009] described that the mean characteristics of the SASH may change due to the passage and eventual permanence of cyclones, troughs, vortices, and frontal systems. This was the situation found during T3 as shown in Figures 3i and 3j, held between 15 June 10:50h local time and 17 June 2012 00:20h local time from east to west. The atmospheric conditions are marked by the formation of an extra

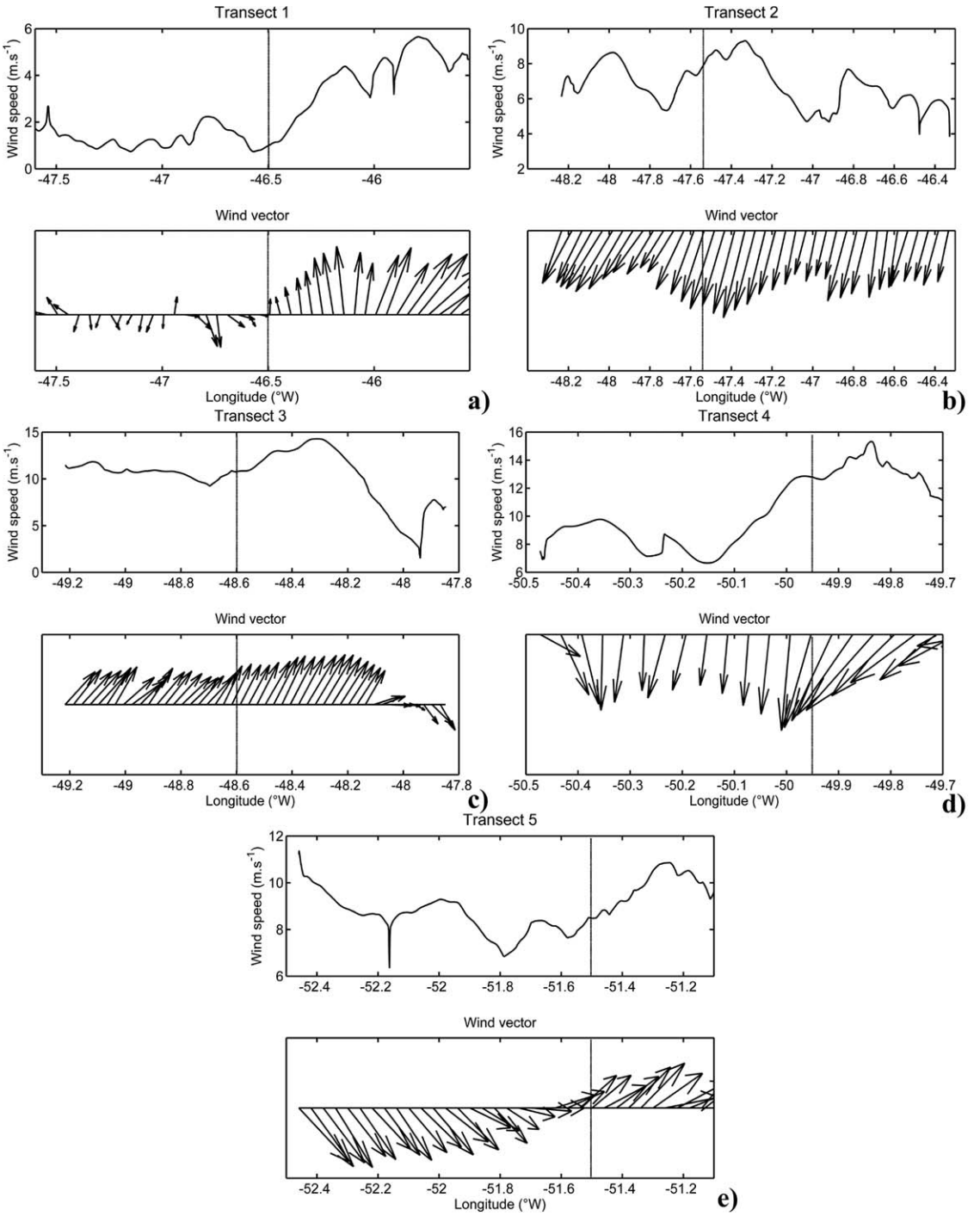

Figure 4. Wind speed (m.s^{-1}) and wind direction at transects T1–T5.

tropical cyclone in open ocean south of T3 with centered at around 40°S, 36°W. This cyclone has drastically changed the predominant wind direction to come from the south (Figures 3k, 3l, and 4c). Wind intensities arose from ~4 m.s^{-1} to a peak close to 15 m.s^{-1} and then stabilized at around 11 m.s^{-1}. As a consequence, an accentuated cold advection with values ranging from 6°C.d^{-1} to −8°C.d^{-1} was found over T3 (Figure 3l).

The T4, was held between 17 June 22:10h local time to 18 June 2012 09:30h local time from east to west. This transect (T4) was marked by the formation of an extra tropical cyclone south of the SBCS. This system

is easily seen in the sea level pressure chart (Figure 3m) as low pressure system, with 1004 hPa in its center. It is also observed as a cloudy band with cyclonic curvature in the visible (and infrared, not shown) satellite images analyzed here (Figures 3n). Wind intensities dropped from ~14 m.s^{-1} to ~8 m.s^{-1} (Figure 4d). Even with the strong northerly wind component (Figures 3o, 3p, and 4d), the thermal advection was slightly positive (Figure 3p).

Synoptic conditions for T5 that was held between 19 June 09:55h local time and 20 June 2012 01:40h local time from east to west are shown in Figures 3q and 3r. T5 was sampled under the incursion of an intense cold postfrontal situation, dry air mass over the Southwestern Atlantic Ocean (Figures 3s and 3t). This situation was a consequence of a frontal system passage associated to the cyclone described before. During the realization of T5, this cyclone was still present to southeastern of our study area. The satellite image (Figure 3r) shows the presence of shallow cumulus clouds that form in the region as a consequence of the incursion of polar (cold and dry) air mass over the warmer ocean's surface. As the time progressed when traveling with the ship from east to west along T5, the southwestern winds shifted to northeastern winds. Wind intensities dropped at the beginning of T5 from ~11 m.s^{-1} to about 8 m.s^{-1} and then arose again to initial intensities (Figure 4e). A sharp decrease in the air temperature associated with the presence of the cold air mass caused a considerable cold air advection of 10°C.d^{-1} to −12°C.d^{-1} over the area (Figure 3t).

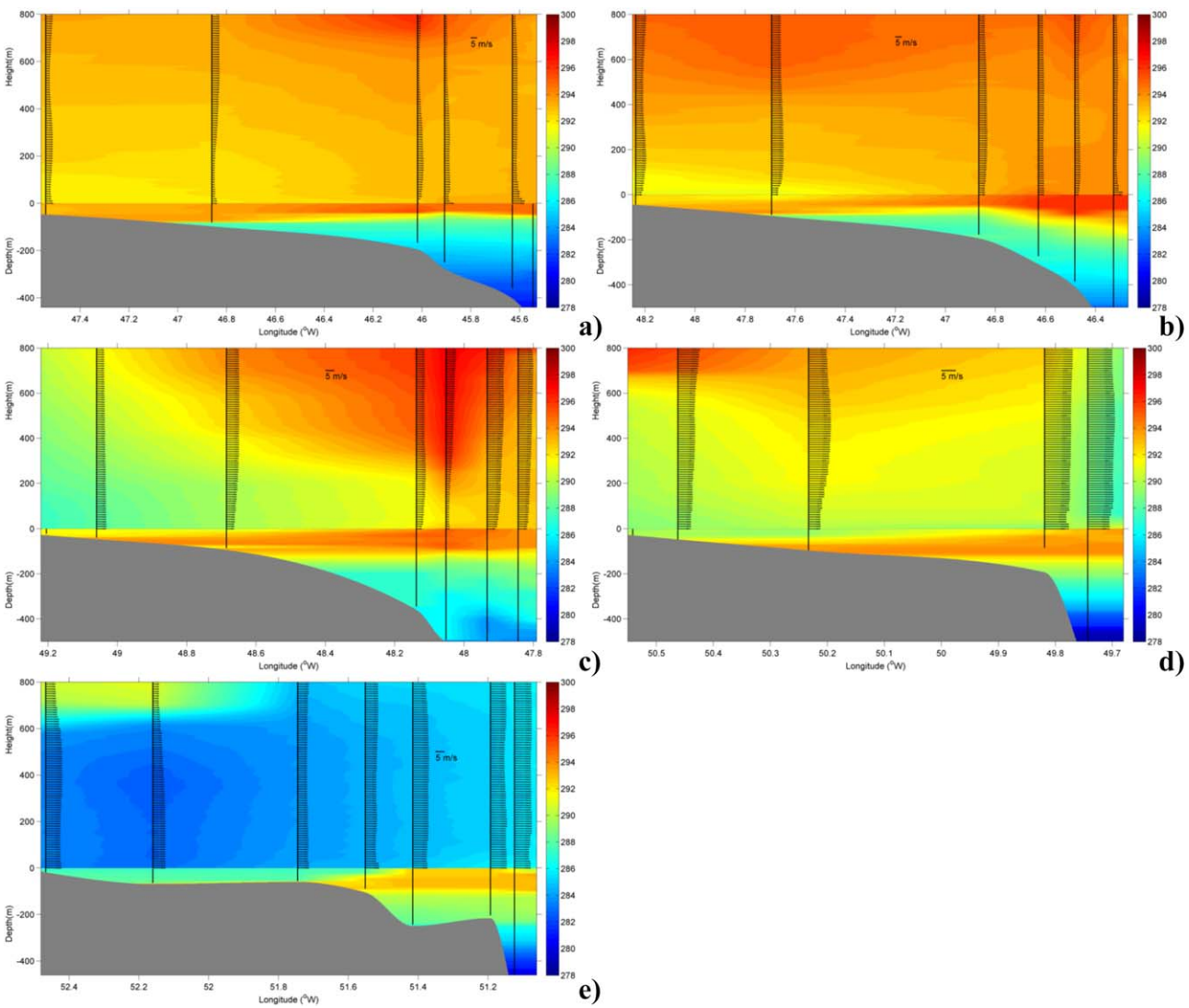

Figure 5. Temperature (K) profiles of the atmosphere and the ocean taken simultaneously using radiosondes and XBTs along the RV *Cruzeiro do Sul*'s route from T1 to T5 (a–e, respectively). Zonal wind vectors (m.s^{-1}) are also displayed.

3.2. MABL and Ocean's Thermal Gradients

Figure 5 presents a synoptic snapshot of the thermal structure of the MABL and ocean mixed layer made for each transect analyzed here at the temporal average of the transect's duration of sampling. The figure is similar to the ones presented by *Pezzi et al*. [2005, 2009] for the BMC region to show the impacts of the lateral SST gradients of the BMC region on the air potential temperature (θ_{air}) and wind magnitude of the atmosphere just above the sea at the synoptic meteorological temporal scale. In order to produce this figure, we followed *Pezzi et al*. [2005, 2009] approach, using radiosonde and XBT data. This figure is the first of its kind made for the SBCS region.

When presenting this XBT data, we do not intend to extensively discuss the hydrography of our study region. Instead, we only describe the main water temperature distribution along transects T1 to T5 that is important to the MABL analysis. The ocean's vertical thermal structure shows that during the realization of the ACEx/SIMTECO cruise, the thermocline was between 50 and 100 m. In most of the transects to the exception of T5 (Figure 5e), the cross-shelf thermal gradients seen between BC and BCC were not very accentuated. Together with the change in salinity, these thermal contrasts indicate the BC/BCC front. Although the BC/BCC front may be identified with the STSF, the absence of the Subantarctic Shelf Water (SASW) in most of our study area and period suggests that this proper shelf front was located southward. Our front here is mainly between PPW and TW.

Generally speaking, Figure 5 shows that in the offshore region where higher SST (BC) waters are located the air temperature and wind magnitude at the sea surface are equally higher. Ocean-atmosphere turbulent heat fluxes, as a consequence (Figures 8a and 8b) are also higher over BC waters. Figures 5a and 5c clearly show that the SST influences the MABL vertical structure: over warm, BC waters the atmosphere is warmer and presents stronger winds at the sea surface. On the contrary over cold, LPP waters the atmosphere at its lower levels is colder with weaker winds. The MABL, however is not always well mixed (unstable) with a small vertical wind shear over warmer waters or the contrary over colder waters as classically expected for the SST forcing through the static stability mechanism [*Wallace et al*., 1989]. As discussed later on this paper, differences from the classical adjustment models are consequence of the presence of cyclogenesis and atmospheric frontal passages in our study area.

Although the cross-shelf SST gradient between BCC and BC were not very accentuated in T1 and T2 (Figures 5a and 5b), there is a considerable θ_{air} gradient on the cold side of the BC/BCC front in comparison to the warm side. In terms of the wind speed, we can note a larger vertical wind shear over the BC waters with higher winds at the sea surface in the eastern more radiosonde stations, indicating instability but not good mixture along the entire MABL vertical column. Still over BC waters, 3 radiosonde profiles located in longitudes from 47°W to 46.4°W are classical profiles of MABL static stability adjustment to high SST with turbulent mixing from surface to 800 m height (Figure 5b).

The atmosphere in T3 (Figure 5c) presents an intense vertical gradient of θ_{air} especially at the warm side of the BC/BCC where higher θ_{air} is observed in heights over 200 m. As warm air is located on top of cold air, the atmosphere is stable although a small vertical wind shear is still present at layers close to the sea surface. In T4 a strong vertical gradient of θ_{air} is located at the cold side of the BC/BCC although higher θ_{air} is observed in the MABL only in heights over 600 m. Across-shore SST gradients are more intense between LPP and BC waters in T4 (Figure 5d) and the atmosphere is more turbulent, well mixed over the warm side of the oceanographic front.

The highest horizontal SST contrast between BC and BCC waters were found along T5 (Figure 5e). The θ_{air} vertical profile shows a thicker MABL at the warm side of the front, although at both sides of the front the MABL is well mixed. Such well-mixed conditions affect mean wind speed, which is observed to be uniform throughout the MABL extension above BCC waters. Increased wind shear happens at higher levels. Although high, the across-shore SST contrasts of the BC/BCC front are not directly playing a strong influence in the atmospheric turbulence probably because of the influence of the cyclone described in section 3.1.

3.3. MABL Stability and In Situ Atmospheric Sea Level Pressure Forcing

In this section, atmospheric sea level pressure (SLP) and sea level air temperature (T_{air}) and SST data from the ship's thermosalinographer data collected by the high-frequency sensors of our micrometeorological are used to directly compare SLP with the static stability parameter. This is defined as SST-T_{air}. All of our

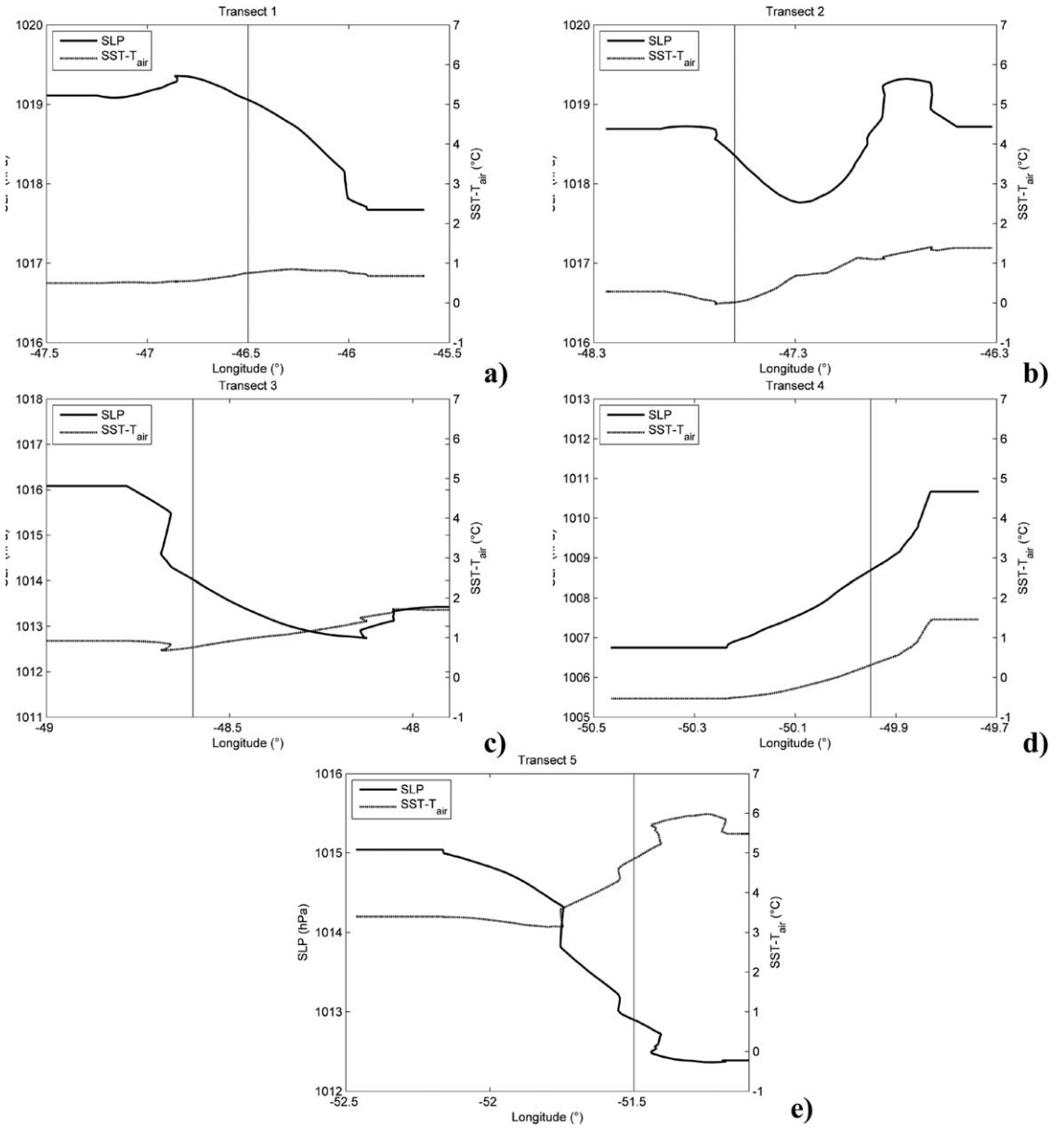

Figure 6. Synoptic, in situ measurements of SLP (hPa) and SST − T_{air} (°C) taken along the ACEx/SIMTECO across-shore transects T1–T5 (a–e, respectively). The vertical line denotes approximately the BC/BCC front position.

high-resolution meteorological measurements including SLP are in good agreement with the lower-frequency AWS data (not shown here).

This investigation is made in order to evaluate the hypothesis of *Lindzen and Nigam* [1987] that the surface winds, dependent upon the SLP lateral gradients, are modulated by the hydrostatic adjustment of the MABL stability. SST-T_{air} and SLP high-frequency data for all transects are presented in Figure 6. As discussed by many authors in open ocean areas of the World Ocean [*Pezzi et al*., 2005, 2009; *Small et al*., 2008; *Camargo et al*., 2010; *Kilpatrick et al*., 2014], the hydrostatic adjustment hypothesis lead us to expect lower (higher) SLP values over warmer (colder) waters. However, this can only be the case when the analyzed region is neither under a strong atmospheric synoptic system action nor in the presence of a crossing, strong horizontal atmospheric advection.

Table 2. MABL Top Heights at the Warm and Cold Side of the BC/BCC Front at Each Transect

Transect	h_0 at the Warm Side (m)	h_0 at the Cold Side (m)
T1	700	1000
T2	1300	1100
T3	800	790
T4	800	630
T5	900	630

This expected situation was present in all transects except during some time over warm waters in T2 and in T4 (Figures 6b and 6d). The decrease in SLP values was between 1 and 3 hPa from the cold to the warm side of the BC/BCC front. The reverse pattern observed in T4 (rising of about 4 hPa from the cold to the warm side of the BC/BCC front) suggests that the local, SST-induced modulation of the MABL was not superimposing its signal over the signal of the large-scale synoptic system (the extratropical cyclone discussed in section 3) present at T4 region while the ship was sailing there. Evidence of the superimposed large-scale signal over the local MABL modulation is seen in Figure 6d where lower SLP values of ~1006 hPa are observed over the cold waters of SST close to 16.5°C. On the other side of the BC/BCC front SLP rises up to 1011 hPa approximately over warm waters of about 20°C. Nonetheless, this analysis shows that the local SST even on small spatial scales (like the one of the SBCS in respect to other areas of the World Ocean) may cause the hydrostatic adjustment of the MABL. As expected though, the local hydrostatic MABL modulation caused by SST is lost in the presence of a transient atmospheric system crossing the region.

The cross-shore distribution of the static stability parameter SST-T_{air} along the transects analyzed here (Figure 6) demonstrates that, except for T4 over cold waters, SST was always warmer than the air temperature, leading to positive values (unstable MABL). Typical values of SST-T_{air} were about 1–2°C except during some time over warm waters in T5 when values reached ~6°C. It is worth to remember that when SST-T_{air} is positive we have turbulent heat transferred from the ocean to the atmosphere.

3.4. Vertical Structure of the MABL

In order to analyze the impact of the SST bottom boundary condition on the vertical structure of the MABL in our study area, we followed the same strategy used by *Pezzi et al*. [2009]. The authors computed mean vertical profiles of many meteorological variables to describe the MABL in both cold and warm sides of the BMC region in the Southwestern Atlantic Ocean. For each transect performed during the ACEx/SIMTECO cruise, we used data of all stations taken over LPP waters in the coastal zone to make average profiles of the MABL on top of the BCC, the cold part of the BC/BCC front. Equally, we averaged data of all sites taken over BC waters to characterize the MABL condition on top of the warm part of the BC/BCC front. The variables used here to describe the differences between the cold and warm part of the BC/BCC front, as in *Pezzi et al*. [2009], were the θ_{air}, the atmospheric mixing ratio or specific humidity (q) and the relative humidity (RH).

In order to assess the MABL top height (h_0), we can assume that θ_{air} and q are well mixed within the MABL and remain approximately constant (adiabatic) in the mixed layer. MABL height depends on the turbulent mixing [*Stull*, 1998]. A strong gradient of θ_{air} and q is observed at higher levels of the atmospheric profile when the inversion layer is reached.

After that level, the point that determines the inversion layer and h_0 is where an abrupt change occurs on the profiles, with θ_{air} increasing and q decreasing [*Fisch et al*., 2004]. For each of the transects described here, the mean MABL top height (h_0) at each side of the BC/BCC front was subjectively determined in the average θ_{air} and q profiles as the height where the capping inversion layer or entrainment zone were located. The number of radiosondes profiles used at each side of the BC/BCC front to compute the h_0 averages are described in Table 1. The resulting mean values of h_0 at the warm and cold sides of the front for each transect are indicated in Table 2. The h_0 difference between the warm and cold sides of the front in all transects is also seen in Table 2. In all cases, h_0 is deeper at the warmer side, with the important exception of T1. In this case, there is a shallow stable layer near the surface at the warmer side, which we speculate to be caused by advection of warmer continental air toward that region. It is possible that such stable layer near the surface opposes the growth at the MABL at the warm side, causing it to be shallower than at the colder side. From this table, we notice that T1 and T3 presented a considerably thicker MABL at the cold side of the BC/BCC front while in the other transects the inverse occurred.

Figure 7 presents the averaged vertical profiles of θ_{air}, q, RH taken with data of all transects at each side of the BC/BCC front. The analysis is restricted to the first 2000 m below which the MABL is located (Tables 1 and 2). Below h_0 at both warm and cold sides of the front, we do not observe any accentuated gradient for temperature, humidity, and wind, except very close to the sea surface where instrumental adjustment of the radiosonde sensors is more critical. Figure 7 shows a MABL well developed and mixed at both sides of the front. The atmospheric variables in the MABL show a well-defined, convective MABL structure. As also noticed over warm waters of the BMC region by *Pezzi et al*. [2009], we observe that over the warm side of the BC/BCC front we have a well-developed and mixed MABL with a higher h_0 when compared to the cold

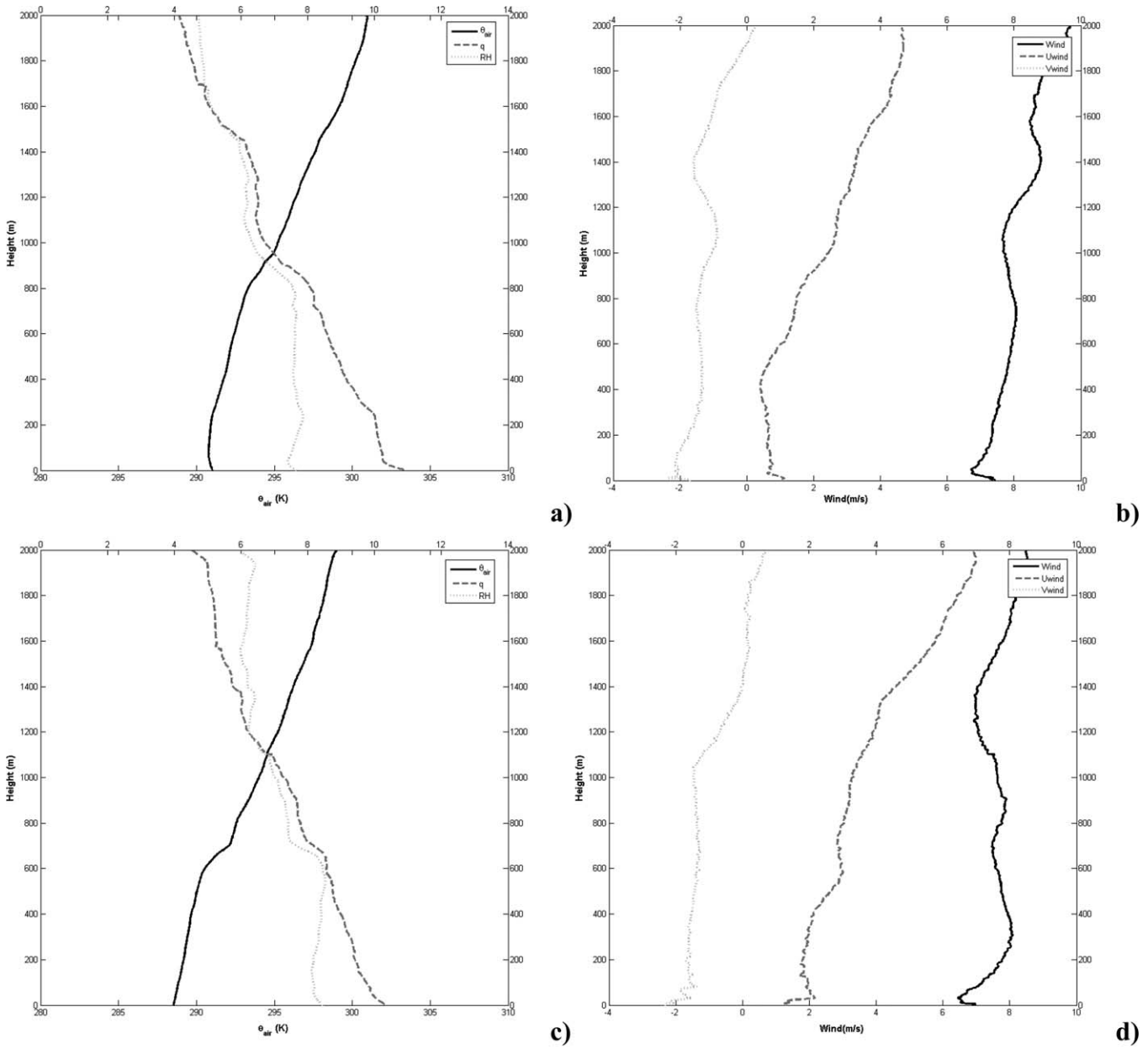

Figure 7. (left) Mean vertical profile of θ_{air}, q, and relative humidity, (right) zonal (u) and meridional (v) wind components and wind magnitude over warm, (top) BC waters and (bottom) over cold, BCC waters. MABL top is 900 m at the warm side and 600 m over cold side of the front, approximately. The RH profiles were divided by 10^{-1} in order to plot q values in the same order of magnitude.

side front. The vertical distribution of the atmospheric variables in the MABL over cold waters (Figures 7c) displays a MABL top a bit thinner in comparison to the warm side. However, a capping inversion presented by the RH is at about 600 m.

Apart from the first ~50 m off the sea surface, the humidity increases with height on both sides of the BC/BCC front, reaching values near to 90% at the capping inversion. Above h_0 there is an accentuated decrease in humidity to values near to 50% (warm side, Figure 7a) and 40% (cold side, Figure 7c). Above the first inversion level, q decreases and remains almost constant up to a secondary inversion level, which is detected at 900 m on the cold side of the front (Figure 7c). The vertical structure of the inversions observed in the RH and q profiles indicates a strong reduction of moisture, which originates at the sea surface and ascends toward the MABL. This fact suggests that the upper MABL is decoupled from the surface layer.

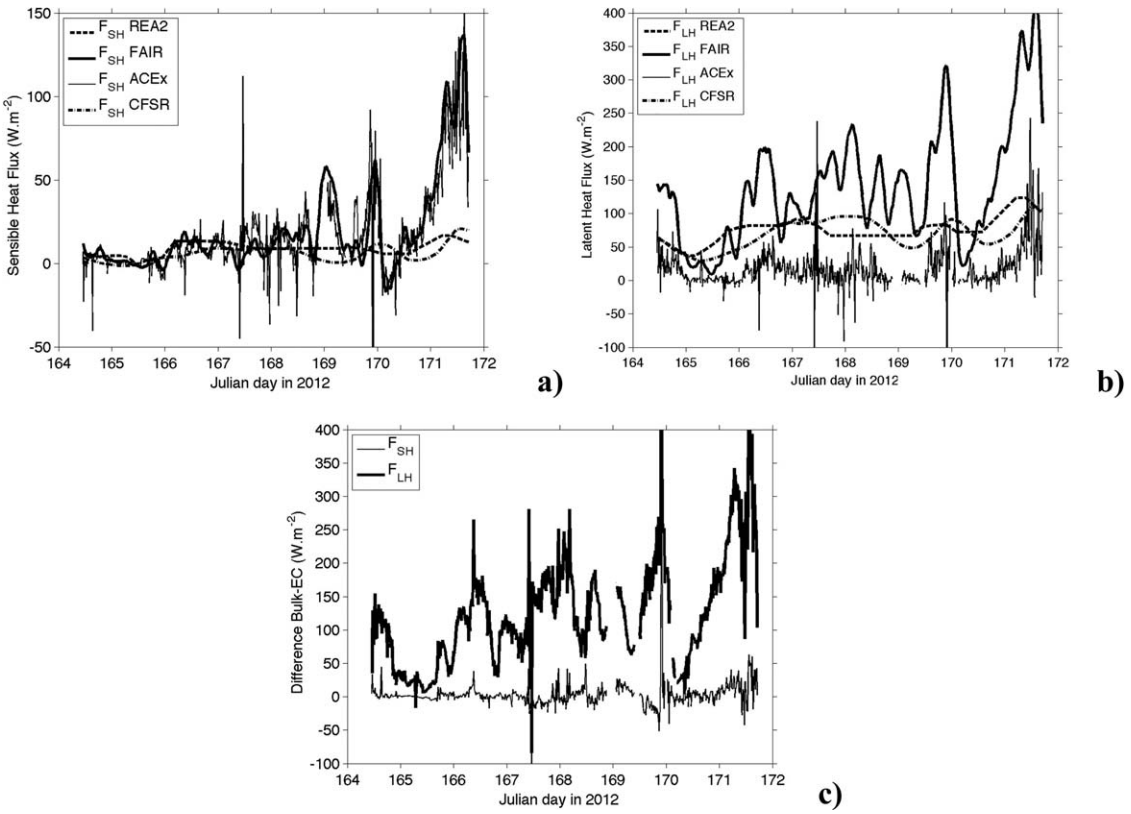

Figure 8. Heat fluxes estimated by Eddy Covariance (ECM) and bulk methods. (a) Sensible heat fluxes; (b) latent heat fluxes, (c) difference bulk-EC of sensible (SH), and latent (LH) heat fluxes. The time series spans over the whole cruise period from 12 to 21 June 2012 (Julian days 164–172). The acronyms used in Figures 8a and 8b legends are REA2, for NCEP reanalysis version 2, FAIR, for Fairall bulk formula, ACEx, for EC data and CFSR, for NCEP Climate Forecast System Reanalysis.

Hashizume et al. [2002] observed a similar pattern over cold waters at the eastern Equatorial Pacific while *Pezzi et al*. [2009] noticed the same at cold side of the BMC. Below h_0 at both sides there is not any accentuated gradient (except below 10 m approximately) for temperature, humidity, and wind.

The vertical profiles of the wind reveal interesting features. We notice in both sides of the front that the prevailing winds are stronger at the sea surface on the cold side of the front. The zonal component of the wind (u) was particularly high (near 4 $m.s^{-1}$) in average over cold at heights of about 10 m from the sea level (Figure 7d). The mean wind magnitude profiles over the BC and BCC regions (Figures 7b and 7d, respectively) are very similar ranging from 7 to 9 $m.s^{-1}$.

3.5. Sensible and Latent Heat Fluxes

In this section, we analyze the ocean-atmosphere heat fluxes measured directly by the sensors mounted at our micrometeorological tower in the ship's bow and determined by the Eddy Covariance. These data are compared with fluxes estimated through the bulk parameterization proposed by *Fairall et al*. [1996]. These data are compared to the heat fluxes derived from two different reanalysis data set, which are NCEP 2 and CFSv2. For the reanalysis data, it was performed an average in time during the cruise period (12–20 June 2012) and after extracted the heat flux values at the same spatial position where EC measurements were presented here. This is not an objective and in depth comparison, instead it is used to have an idea if EC and bulk fluxes estimated are approximately in the same order of magnitude. This bulk parameterization was first developed to be used in conditions of weak to moderate winds and subsequently modified to include stronger winds in the version known as COARE 3.0 [*Fairall et al*. 2003]. *Pezzi et al*. [2005, 2009] employed this scheme to in situ data collected at BMC region and can be referred for details of the parameterization (bulk) flux methodology calculation and limitations. The turbulent latent and sensible heat fluxes are one of the ways by which energy is exchanged between the ocean and the atmosphere. Therefore their

Table 3. T_{air}, SST, Sensible (*SH*), and Latent (*LH*) Heat Fluxes Averages Over the Warm and Cold Sides of the BC/BCC Front at Each Transect Made During the ACEx/SIMTECO Cruise[a]

	BC (Warm)				BCC (Cold)			
Transect	T_{air} (°C)	SST (°C)	*SH* (W.m^{-2})	*LH* (W.m^{-2})	T_{air} (°C)	SST (°C)	*SH* (W.m^{-2})	*LH* (W.m^{-2})
T1	21.6	22.3	3.8 ± 3.5	24.8 ± 16.5	20.5	21.0	0.5 ± 1.5	2.6 ± 6.5
T2	21.9	22.8	7.4 ± 5.1	21.3 ± 17.7	19.7	19.9	−2.7 ± 4.3	−0.5 ± 5.3
T3	20.2	21.2	12.7 ± 10.8	10.4 ± 18.9	17.4	19.2	17.4 ± 14.7	7.9 ± 16.9
T4	17.9	19.6	39.1 ± 40.0	35.6 ± 51.4	17.5	16.9	−8.0 ± 5.4	−2.6 ± 6.8
T5	13.6	19.1	84.4 ± 33.9	65.5 ± 47.2	11.8	15.0	32.9 ± 10.1	17.7 ± 19.0

[a]The heat fluxes were calculated by the Eddy Covariance method and are presented with their respective standard deviations.

correct determination is crucial to well understand the effects of the ocean-atmosphere interactions on the weather and climate of the South Atlantic Ocean and its vicinity.

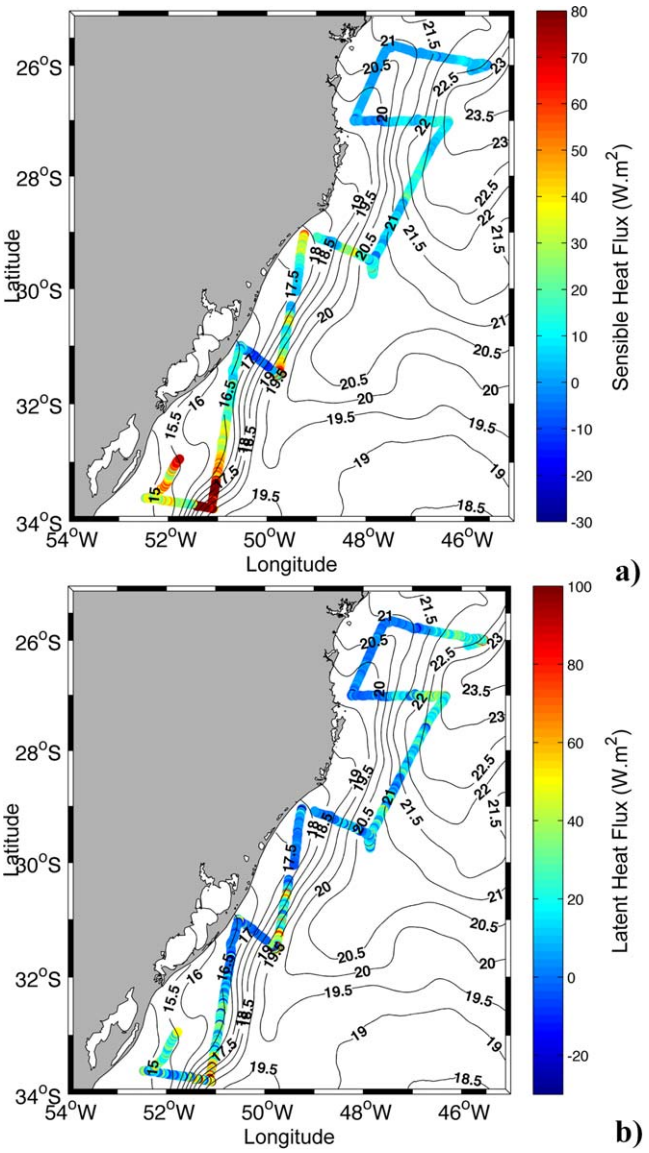

Figure 9. Spatial distribution of (a) latent and (b) sensible heat fluxes (W.m^{-2}) between the ocean and the atmosphere during the ACEx/SIMTECO cruise. Isolines represent the mean SST for June based on satellite data.

These fluxes are proportional to the temperature (specific humidity) gradient between the air and the sea surface, to the wind magnitude and to a stability coefficient. The temporal distribution of the sensible (F_{SH}) and latent (F_{LH}) heat fluxes estimated by the EC and parameterization methods during the ACEx/SIMTECO cruise is shown in Figures 8a and 8b. Positive values indicate heat fluxes from the ocean to the atmosphere and negative ones indicate the opposite. For better visualization, we applied a 2 h-averaged moving window filter on our original time series data. Figure 8a shows that the temporal variability of F_{SH} is quite similar when EC and parameterization methods are compared. This variability is dominated by semidiurnal cycles probably related to the diurnal heating and cooling of the lower atmosphere. Higher differences in the order of 10–20 W.m^{-2} are observed in F_{SH} magnitude during the period between Julian days 166–169 (14–17 June). There is a noticeable trend in the F_{SH} magnitude throughout the sampling period when values rise from about 0–40 W.m^{-2} from the beginning to the end of the series when the vessel went from north toward the south of our study region. A peak occurred during Julian day 171 (19 June) when F_{SH} magnitudes reached ∼80 (EC) to ∼100 W.m^{-2} (bulk). This event of 19 June 2012 is probably related to the incursion of a postfrontal cold, dry air mass over the Southwestern Atlantic Ocean which was associated to the cyclone described in section 3.1 of this paper (Figures 3i and 3j). F_{SH} magnitude averages over

the entire period are 18.8 and 14.5 W.m^{-2} with standard deviations of 26 and 20 W.m^{-2} for the EC and bulk methods, respectively. The mean F_{SH} magnitude bias (difference) of the bulk compared to EC method was −4 W.m^{-2}.

Although the F_{LH} variability estimated by the EC and bulk methods is similar throughout the study period (dominated by the semidiurnal cycle just as the F_{SH}), their magnitudes differ substantially (Figure 8b). It is clear that the bulk method super estimates F_{LH} when compared with EC method. The F_{LH} magnitude averages for the study period are 18 W.m^{-2} and 78.3 W.m^{-2} with standard deviations of 29.3 W.m^{-2} and 53.5 W.m^{-2} for the EC and bulk methods, respectively. The mean F_{LH} magnitude bias of the bulk compared to EC method was 60 W.m^{-2} although it reached extremes of 180–210 W.m^{-2} during Julian day 171 (19 June) when our study area was under a strong cold air advection caused by the postfrontal system situation, as discussed in section 3.1.

On the other hand, the EC and reanalyzes comparison clearly shows that for the large part of cruise the heat fluxes measured are in a good agreement, mainly for the F_{SH} (Figure 8a). That is the when EC and bulk fluxes are compared to both reanalyzes data set. An exception to that occurs during the two last days when these values are considerably larger (compared to reanalyzes data) that may be caused by the cold air advection. Atmospheric condition described above. The F_{LH} values are underestimated when compared to the reanalysis products; however, they are close on order of magnitude (Figure 8b). F_{LH} compares better to the CFSv2 pattern. However, it is interesting to note that F_{LH} derived from bulk flux parameterization is at least one order of magnitude above the reanalysis fluxes over some regions. Similar findings are shown by *Rouault et al*. [2003], when they used *Fairall et al*. [1996] to estimate heat fluxes using in situ data collected during an oceanographic over the Agulhas Current warm core, and compared those estimations with ECMWF and NCEP heat fluxes reanalysis. An intercomparison of six different heat fluxes data set analyzed by *Yu et al*. [2011] to the Southern Ocean showed that the larger variances and differences are found to the latent heat flux and suggest that what may cause the larger spatial variability among the data sets are the sea-air specific humidity and temperature differences.

The nature and driving mechanisms responsible for the bias between reanalysis, EC, and bulk estimations made here of heat fluxes are subjects beyond the scope of the present paper. Although the amplitude of the bias may be related to the synoptic conditions of the atmosphere at the ocean-atmosphere interface, we did not investigate the main variable causing the differences between the heat fluxes estimated here by the two methods. Owing to the importance of the heat flux estimated for derived variables and for the weather and climate prediction, this issue needs a specific investigation that should look carefully through our in situ measurements technique and the calculations used for determining the turbulent transfer coefficient used in the COARE 3.0 parameterization scheme which is based on turbulent transfer coefficients of momentum and humidity [*Fairall et al*., 1996, 2003] as well as comparing more in depth with other reanalysis data set. It is worth to say that the COARE algorithm is regularly updated and refined. Newer versions of the algorithm can be used over a diversity of synoptic atmospheric and sea state conditions (as function of low and high wind speeds). An update of COARE is reported in *Edson et al*. [2013] where a refined version named COARE 3.5 is presented. A wide range of distinct environmental conditions (sea state, wind speed, and atmospheric stability for example) is used in order to improve the parameterizations of drag coefficients over the ocean.

Table 3 presents the T_{air}, SST, F_{SH}, and F_{LH} averages over the warm and cold sides of the BC/BCC front at each transect made during the ACEx/SIMTECO cruise. The table considers only the heat fluxes computed by the EC method. Despite two cases in transects T2 and T4 over cold waters where F_{SH} and F_{LH} averages were negative, all the other average heat fluxes presented positive values over either warm or cold waters. There is a noticeable tendency of the averaged heat fluxes to increase from T1 toward T5, or from the beginning toward the end of the field experiment between 12 and 21 June 2012. Positive heat fluxes occur when SST is larger than T_{air}. This was the case in all situations apart from T4 over cold waters (Table 3). This indicates that the sea surface acts as a heat source to the atmosphere. Table 3 also shows that there is a difference in the magnitude of the total heat fluxes ($F_{SH} + F_{LH}$) between the cold (BCC) and warm (BC) sides of the front. The total heat fluxes summed up to 3.1 W.m^{-2} (cold side) and 28.6 W.m^{-2} (warm side). The flux exchanges were more intense on the warm side, and there was a small reduction in heat energy release to the atmosphere at cold side of the BC/BCC front. Our results corroborate the fact that the heat transfer between the ocean and the atmosphere tends to decrease over colder

waters of the South Atlantic Ocean as previously described by *Piva et al*. [2011], *Silva Dias et al*. [2004], and *Pezzi et al*. [2005, 2009].

Transect T5 shows an interesting situation where the sampling region was under the influence of a post-frontal air mass, where the air temperature was very low (refer to section 3.1 of this paper). The heat flow is positive in both front sides and the SST is higher than T_{air} (Table 3) for the whole transect. Because of that, this was the largest difference ($T_{air} - SST$) seen in all transects sampled during the ACEx/SIMTECO cruise. In transect T5, the highest difference ($T_{air} - SST$) occurs over the BC, resulting in a total heat flux magnitude almost three times bigger at the warm side of the front (total heat flux of 149.9 W.m^{-2}) compared to the cold one (total heat flux of 50.6 W.m^{-2}).

Figure 9 presents the spatial distribution of the F_{SH} and F_{LH} fluxes between the ocean and the atmosphere during the ACEx/SIMTECO cruise based on data obtained by the micrometeorological tower using the EC method. Remembering that the micrometeorological tower was working throughout the entire period when *RV Cruzeiro do Sul* was at sea, recordings were made not only during transects T1–T5 but also on route between them. Figure 9 indicates a clear modulation of the SST spatial variability on the heat fluxes distribution and the energy partition between F_{SH} and F_{LH} fluxes. As previously seen in Figure 8, most of the time both F_{SH} and F_{LH} fluxes were positive, although close to zero or negative (especially *SH*) sometimes.

Comparing Figure 9 with Figure 2 (SST and SST zonal gradients distribution), we notice that as well as higher toward the south of the study region, F_{SH} and F_{LH} fluxes also tend to be higher at the location of the higher SST zonal gradients that mark the BC/BCC front. Figure 9 indicates that the most of the ocean at our study region, during the period of the ACEx/SIMTECO cruise was acting as a source of heat to the atmosphere. This fact is corroborated by the calculation of the average total heat flux ($F_{SH} + F_{LH}$) that resulted in a positive (ocean to the atmosphere) value of $\sim$36 W.m^{-2}. This is an expected situation since the cruise was done during the wintertime, when usually the air is colder than sea surface due to the influence of polar air masses that reach our study region in the south of Brazil associated to the typical climate characteristics of the Austral winter. As discussed before, the incursion of a polar, dry, and cold air mass during the realization of T5 toward the last days of our experiment can explain the extremely high values of F_{SH} and F_{LH} fluxes found in the southernmost part of our study area.

Our results, although restricted to a small area of the coastal region in the south of Brazil, are consistent with previous studies made to other regions characterized by strong oceanic thermal gradients. Most of these studies suggest that the atmosphere tends to adjust itself to the narrow oceanic fronts, where the MABL experiences a vertical stratification transition from an unstable condition over warm waters to a stable condition over cold waters [e.g., *Chelton et al*., 2001; *Hashizume et al*., 2002; *Xie*, 2004; *Tokinaga et al*., 2005; *Pezzi et al*., 2005, 2009; *Small et al*., 2008; *Kilpatrick et al*., 2014].

We believe our results provide strong evidences that the surface processes occurring at the South Brazilian Continental Shelf during wintertime are crucial for modulating the heat fluxes and the MABL stability processes at this region. The evidences of the inversion or reduction (increase) of the heat fluxes over the cold (warm) waters presented here are consistent with the MABL stability mechanisms described in previous studies [*Lindzen and Nigam*, 1987; *Hayes et al*., 1989; *Wallace et al*., 1989, *Hashizume et al*., 2002].

4. Conclusions and Final Remarks

Many aspects regarding the MABL modulation by oceanic thermal gradients are not yet fully understood. This study demonstrated that the across-shelf thermal gradients found between the waters carried by the BC and the BCC during winter play a significant role on the MABL modulation and stability along the Southern Brazilian Continental Shelf. Although weaker than other thermal gradients found elsewhere in the Global Ocean such as the BMC region [*Pezzi et al*., 2005, 2009], the Gulf Stream [*Minobe et al*., 2008], and the Kuroshio [*Xu et al*., 2010, 2011; *Tanimoto et al*., 2011], the thermal gradients off the SBCS are strong enough to produce a local atmospheric modulation. The heat fluxes between the ocean and the atmosphere are equally dependent on the local SST gradients but at the same time affected by the atmospheric synoptic conditions typical of the wintertime at subtropical latitudes of the southern hemisphere. To our knowledge, this is the first time in the literature when the synoptic atmospheric conditions in the South Atlantic are reported to affect the coastal fluxes between the

ocean and the atmosphere. The fluxes were measured in the SBCS using the EC method. Previous applications of the method in the northern hemisphere were reported in *Miller et al*., [2008]. Although not intending to find the physical phenomena responsible for that, we compared sensible and latent heat flux data estimated by both the EC method and the commonly applied parameterization (bulk) scheme proposed by *Fairall et al*. [1996, 2003] and (NCEP 2, CFSv2) reanalysis data. Our results showed that in general EC has showed a good agreement with the reanalysis data, mainly with CFSv2. That was the case for F_{SH}. An exception to that was seen when the sampling was made during postfrontal cold advection situation, where both F_{SH} EC and bulk values are considerably larger (compared to reanalyzes data). For the F_{LH}, EC followed similar pattern to the CFSv2, however underestimating values.

The heat fluxes between the ocean and the atmosphere in the SBCS region behave similarly to other observations described for the larger, neighbor frontal region of the South Atlantic Ocean in the Brazil-Malvinas Confluence [*Pezzi et al*., 2005, 2009; *Acevedo et al*., 2009; *Camargo et al*., 2013]. Although SST gradients are weaker than those of the BMC, the ones found during wintertime at the SBCS are equally important being able to locally modulate the MABL stability, heat, and CO_2 fluxes. This is a point to be further investigated in order to improve regional weather and climate forecast models.

On some transects sampled by *RV Cruzeiro do Sul* during the ACEx/SIMTECO campaign, it was possible to observe stronger surface winds associated with an unstable MABL over warm (BC) waters. On this side of the BC/BCC front, a reduction in the wind shear and a decrease in the static stability of the near-surface atmosphere are also seen. Over the cold side of the front, on the other hand, the MABL was more stable, the wind shear was stronger, and the surface winds were weaker. Those signatures are consistent with the static stability mechanism proposed by *Wallace et al*. [1989]. Still over cold waters, the atmosphere presents an increased vertical wind shear and a weakening of the surface winds. Simultaneously, the hydrostatic stability mechanism proposed by *Lindzen and Nigam* [1987] was often present: lower (higher) atmospheric sea level pressure was seen over warmer (colder) waters. Nearly all aspects of the ocean-atmosphere coupling observed in our results are in agreement with previous studies made for other oceanic frontal regions previously cited. The combining MABL adjustment model to the local SST fields was also described for the tropics in the eastern equatorial Pacific Ocean [*Wallace et al*., 1989; *Hayes et al*., 1989; *Chelton et al*., 2001; *Hashizume et al*., 2002; *Pezzi et al*., 2004; *Small et al*., 2008; *Spall*, 2007; *Kilpatrick*, 2015].

Even recognizing the value of our results acknowledging that the SBCS waters may act as a modulation mechanism to the MABL stability and heat fluxes, we are also aware that more research is needed to fully understand the differences found between the heat flux measurements and estimations. At the same time, it is also evident that the continuity of sampling this region with good quality data will allow us to collaborate on improve the bulk flux parameterizations for the extra tropical oceanic region. As showed in *Piva et al*. [2011], heat fluxes are a key component to the cyclones development and enhancement in Southwest Atlantic, which is a cyclogenetic [*Gan and Rao*, 1991] and storm track area [*Hoskins and Hodges*, 2005]. Thus the high-resolution (both vertical and horizontal) sampling can lead to improvement on understanding about the surface ocean role on the MABL and the phenomena that take place there.

Acknowledgments

We thank the Brazilian Navy's *RV Cruzeiro do Sul* captain, Com. André Moraes Ferreira and his crew of for their excellent support, friendship, and help on gathering the data during the field survey. The authors acknowledge the Brazilian Ministry of Science, Technology, Innovation and Communication (MCTIC) for making the research cruise possible. We also thank the financial support of the Brazilian funding agencies CNPq to project ACEx (558108/2009–1) and FINEP to project SIMTECO. This is also a contribution to projects 'Advanced Studies in Medium and High Latitudes Oceanography' (CAPES 23038.004304/2014-28) and 'National Institute of Science and Technology of the Cryosphere' (CNPq/PROANTAR 704222/2009). L. P. Pezzi and R. B. Souza are supported by CNPq's fellowships on scientific productivity (CNPq 304633/2012-7 and 308646/2013-4, respectively). A. J. Miller was supported by NSF (OCE1419306). We thank also Dr. A. O. Manzi and the Meteorological Instrumentation Laboratory of Brazilian Center for Weather Forecast and Climate Studies (CPTEC/INPE) for the support with some equipment and for the field campaigns. National Oceanic and Atmospheric Administration (NOAA) and its research units provided reanalysis 2 and CFSv2 (http://www.cpc.ncep.noaa.gov). DHN surface charts can be downloaded from https://www.mar.mil.br/dhn/chm/meteo/prev/cartas/cartas.htm. Infrared images used here are GOES-12 from the CPTEC/INPE can be accessed in http://satelite.cptec.inpe.br/acervo/goes.formulario.logic. All the data for this paper are properly cited and referred to in the reference list.

References

Acevedo, O. C., L. P. Pezzi, R. B. Souza, V. Anabor, and G. Degrazia (2010), Atmospheric boundary layer adjustment to the synoptic cycle at the Brazil-Malvinas Confluence South Atlantic Ocean, *J. Geophys. Res.*, *115*, D22107, doi:10.1029/2009JD013785.

Andrade, K. M. (2005), *Climatologia e Comportamento dos Sistemas Frontais sobre a América do Sul. Dissertação (Mestrado)*, 185 p., Inst. Nacional de Pesquisas Espaciais, São José dos Campos.

Blomquist, B. W., C. W. Fairall, B. J. Huebert, D. J. Kieber, and G. R. Westby (2006), DMS sea-air transfer velocity: Direct measurements by eddy covariance and parameterization based on the NOAA/COARE gas transfer model, Geophys. *Res. Lett.*, *33*, L07601, doi:10.1029/2006GL025735.

Brandini, F. P., A. Scheffer da Silva, E. Teixeira da Silva, and H. Kolm (2007), Sources of nutrients and seasonal dynamics of chlorophyll in the inner shelf off Paraná State—South Brazil Bight, *J. Coastal Res.*, *23*(5), 1131–1140.

Brandini, F. P., M. Nogueira, M. Simião, J. C. U. Codina, and M. A. Noernberg (2014), Deep chlorophyll maximum and plankton community response to oceanic bottom intrusions on the continental shelf in the South Brazilian Bight, *Cont. Shelf Res.*, *89*, 61–75.

Camargo, R., E. Todesco, L. P. Pezzi, and R. B. de Souza (2013), Modulation mechanisms of marine atmospheric boundary layer at the Brazil-Malvinas Confluence region, *J. Geophys. Res. Atmos.*, *118*, 6266–6280, doi:10.1002/jgrd.50492.

Cergole, M. C., S. A. Saccardo, and C. L. Rossi-Wongtschowski (2002), Fluctuations in the spawning stock biomass and recruitment of the Brazilian sardine (Sardinella brasiliensis) 1977-1997, *Rev. Bras. Oceanogr.*, *50*, 13–26.

Chelton, D. B., S. K. Esbensen, M. G. Schlax, N. Thun, M. Freilich, F. J. Wentz, C. L. Gentmann, M. J. McPhaden, and P. S. Schopf (2001), Observations of coupling between surface wind stress and sea surface temperature in the eastern tropical Pacific, *J. Clim.*, *14*, 1479–1498, doi:10.1175/1520-0442(2001)014 < 1479:OOCBSW>2.0.CO;2.

Chelton, D. B., M. G. Schlax, M. H. Freilich, and R. F. Milliff (2004), Satellite measurements reveal persistent small-scale features in ocean winds, *Science*, *303*, 978–983.
Ciotti, Á. M., C. Odebrecht, G. Fillmann, and O. O. Moller (1995), Freshwater outflow and subtropical convergence influence on phytoplankton biomass on the southern Brazilian continental shelf, *Cont. Shelf Res.*, *15*(14), 1737–1756.
Davis, C., and L. F. Bosart (2004), The TT problem, *Bull. Am. Meteorol. Soc.*, *85*, 1657–1662.
Dias, D. F., L. P. Pezzi, D. F. M. Gherardi, and R. Camargo (2014), Modeling the Spawning Strategies and Larval Survival of the Brazilian Sardine (Sardinella brasiliensis). *Progress in Oceanography*, *123*, 38–53, doi:10.1016/j.pocean.2014.03.009.
D'Agostini A, D. F. M. Gherard, and L. P. Pezzi (2015), Connectivity of marine protected areas and its relation with total kinetic energy. *PLoS ONE 10*(10), e0139601, doi:10.1371/journal.pone.0139601.
Edson J. B., V. Jampana, R. A. Weller, S. P. Bigorre, A. J. Plueddemann, C. W. Fairall, S. D. Miller, L. Mahrt, D. Vickers, and H. Hersbach (2013), On the exchange of momentum over the open ocean, *J. Phys. Oceanogr.*, *43*, 1589–1610, doi:10.1175/JPO-D-12-0173.1.
Fairall, C. W., E. F Bradley, J. S. Godfrey, G. A. Wick, J. B. Edson and G. S. Young (1996), Cool-skin and warm-layer effects on sea surface temperature, *J. Geophys. Res.*, *101*(C1), 1295–1308.
Fairall, C. W., E. F. Bradley, J. E. Hare, A. A. Grachev, and J. B. Edson (2003), Bulk parameterization of air-sea fluxes: Updates and verification for the COARE algorithm, *J. Clim.*, *16*(4), 571–591.
Farias, P. C. (2014), Fluxos de calor e dióxido de carbono entre o oceano e aatmosfera na região costeira e oceânica ao sul do Brasil [in Portuguese], master thesis, 91 pp., Universidade Federal de Santa Maria (UFSM). [Available at http://w3.ufsm.br/meteorologia/pos/dissertacoes/29_Priscila_Cavalheiro_Farias_11_07_2014.pdf.]
Fedorova, N. (1999), *Meteorologia Sinótica*, vol.1, Univ. Fed. de Pelotas, Editora Gráfica Universidade Federal de Pelotas (UFPel).
Fisch, G., J. Tota, L. A. T. Machado, M. S. Dias, R. D. F. Lyra, C. A. Nobre, and J. H. C. Gash (2004), The convective boundary layer over pasture and forest in Amazonia, *Theor. Appl. Climatol.*, *78*(1–3), 47–59.
Flügge, M., M. Paskyabi, and J. Reuder (2016), Comparison of direct covariance flux measurements from an offshore tower and a buoy, *J. Atmos. Oceanic Technol.*, *33*, 873–890.
Gan M. A., and V. B. Rao (1991), Surface cyclogenesis over South America, *Mon. Weather Rev.*, *119*, 1293–1302.
Gigliotti, E. S., D. F. M. Gherardi, E. T. Paes, R. B. Souza, and M. Katsuragawa (2010), Spatial analysis of egg distribution and geographic changes in the spawning habitat of the Brazilian sardine Sardinella brasiliensis, *J. Fish Biol.*, *77*(10), 2248–2267.
Guerrero, R. A., A. R. Piola, H. Fenco, R. P. Matano, V. Combes, Y. Chao, C. James, E. D. Palma, M. Saraceno and P. T. Strub (2014), The salinity signature of the cross-shelf exchanges in the Southwestern Atlantic Ocean: Satellite observations, *J. Geophys. Res. Oceans*, *119*, 7794–7810, doi:10.1002/2014JC010113.
Haimovici, M. (1997), *Recursos Pesqueiros Demersais da Região Sul. Avaliação do Potencial Sustentável de Recursos Vivos da Zona Econômica Exclusiva (Revizee)*, editado pela Fundação de Estudos do Mar (FEMAR), 81 pp., Rio de Janeiro.
Hashizume, H., S.-P. Xie, M. Fujiwara, M. Shiotani, T. Watanabe, Y. Tanimoto, W. T. Liu, and K. Takeuchi (2002), Direct observations of atmospheric boundary layer response to SST variations associated with tropical instability waves over the eastern equatorial Pacific, *J. Clim.*, *15*, 3379–3393, doi:10.1175/1520-0442(2002)015 <3379:DOOABL>2.0.CO;2.
Hayes, S. P., M. J. McPhaden, and J. M. Wallace (1989), The influence of sea surface temperature on surface wind in the eastern equatorial Pacific: Weekly to monthly variability, *J. Clim.*, *2*, 1500–1506, doi:10.1175/1520-0442(1989)002 <1500:TIOSST>2.0.CO;2.
Hoskins, B. J. and K. I. Hodges (2005), A new perspective on Southern Hemisphere Storm Tracks, *J. Clim.*, *18*, 4108–4129.
Huebert B. J., B. W. Blomquist, J. E. Hare, C. W. Fairall, J. E. Johnson, and T. S. Bates (2004), Measurement of the sea–air DMS flux and transfer velocity using eddy correlation, *Geophys. Res. Lett.*, *31*, L23113, doi:10.1029/2004GL021567.
Innocentini, V., E. dos Santos, and C. Neto (1996), A case study of the 9 August 1988 south Atlantic storm: Numerical simulations of the wave Activity, *Weather Forecast.*, *11*, 78–88.
Kalnay, E., et al. (1996), The NCEP/NCAR 40-year reanalysis project, *Bull. Am. Meteorol. Soc.*, *77*, 437–470, doi:10.1175/1520-0477(1996).
Kilpatrick T., N. Schneider, and B. Qiu (2014), Boundary layer convergence induced by strong winds across a midlatitude SST front, *J. Clim.*, *27*, 1698–1718, doi:10.1175/JCLI-D-13-00101.1.
Landwehr, S., N. O'Sullivan, and B. Ward (2015) Direct flux measurements from mobile platforms at sea: Motion and air-flow distortion corrections revisited, *J. Atmos. Oceanic Technol.*, *32*, 1163–1178, doi:10.1175/JTECH-D-14-00137.1.
Legey, L. F. L., and S. Jablonski (2004), Quantifying environmental effects on the recruitment of Brazilian sardine (Sardinella brasiliensis), 1977-1993, *Sci. Mar.*, *68*(3), 385–398.
Lentini, C. A., E. J. Campos, and G. G. Podestá (2000), The annual cycle of satellite derived sea surface temperature on the western South Atlantic shelf, *Rev. Bras. Oceanogr.*, *48*(2), 93–105.
Lindzen, R. S., and S. Nigam (1987), On the role of sea surface temperature gradients in forcing low-level winds and convergence in the tropics, *J. Atmos. Sci.*, *44*, 2418–2436, doi:10.1175/1520-0469(1987)044 < 2418:OTROSS>2.0.CO;2.
Lupo, A. R., J. J. Nocera, L. F. Bosart, E. G. Hoffman, and D. J. Knight (2001), South American cold surges: Types, composites, and case studies, *Mon. Weather Rev.*, *129*(5), 1021–1041.
Martins, L. G. N. (2015), Usando a Decomposição em Modos Empíricos para determinação de fluxos turbulentos entre oceano/atmosfera [in Portuguese], PhD thesis, 78 pp., Fed. Univ. of Santa Maria, Santa Maria.
Matano, R. P., V. Combes, A. R. Piola, R. Guerrero, E. D. Palma, P. Ted Strub, C. James, H. Fenco, Y. Chao, and M. Saraceno (2014), The salinity signature of the cross-shelf exchanges in the Southwestern Atlantic Ocean: Numerical simulations, *J. Geophys. Res. Oceans*, *119*, 7949–7968, doi:10.1002/2014JC010116.
Matsuura, Y. (1998), Brazilian sardine (Sardinella brasiliensis) spawning in the southeast Brazilian Bight over the period 1976-1993, *Rev. Bras. Oceanogr.*, *46*(1), 33–43.
McGillis, W. R., J. B. Edson, J. E. Hare, and C. W. Fairall (2001), Direct covariance air-sea CO2 fluxes, *J. Geophys. Res.*, *106*(C8), 16,729–16,745, doi:10.1029/2000JC000506.
McTaggart-Cowan, R., L. F. Bosart, C. A. Davis, E. H. Atallah, J. R. Gyakum, and K. A. Emanuel (2006), Analyses of hurricane Catarina, *Mon. Weather Rev.*, *134*, 3029–3053.
Miller, S., M. Goulden, M. Menton, H. da Rocha, H. de Freitas, A. Figueira, and C. Dias de Sousa (2004), Biometric and micrometeorological measurements of tropical forest carbon balance, *Ecol. Appl.*, *14*, 114–126.
Miller, S., T. Hristov, J. Edson, and C. Friehe (2008), Platform motion effects on measurements of turbulence and air-sea exchange over the open ocean, *J. Atmos. Oceanic Technol.*, *25*(9), 1683–1694.
Miller, S. D., C. Marandino, and E. S. Saltzman (2010), Ship-based measurement of air-sea CO2 exchange by eddy covariance, *J. Geophys. Res.*, *115*, D02304, doi:10.1029/2009JD012193.
Minobe, S., A. Kuwano-Yoshida, N. Komori, S.-P. Xie, and R. J. Small (2008), Influence of the Gulf Stream on the troposphere, *Nature*, *452*, 206–209.

Möller, O. O., Jr., A. R. Piola, A. C. Freitas, and E. J. D. Campos (2008), The effects of river discharge and seasonal winds on the shelf off southeastern South America, *Cont. Shelf Res.*, *28*(13), 1607–1624, doi:10.1016/j.csr.2008.03.012.
Palma, E. D., R. P. Matano, and A. R. Piola (2008), A numerical study of the Southwestern Atlantic Shelf circulation: Stratified ocean response to local and offshore forcing, *J. Geophys. Res.*, *113*, C11010, doi:10.1029/2007JC004720.
Palóczy, A., I. C. A. da Silveira, B. M. Castro, and L. Calado (2014), Coastal upwelling off Cape São Tomé (22 S, Brazil): The supporting role of deep ocean processes, *Cont. Shelf Res.*, *89*, 38–50.
Pedreros, R., G. Dardier, H. Dupuis, H. C. Graber, W. M. Drennan, A. Weill, C. Guérin, and P. Nacass (2003), Momentum and heat fluxes via the eddy correlation method on the R/V L'Atalante and an ASIS buoy, *J. Geophys. Res.*, *108*(C11), 3339, doi:10.1029/2002JC001449.
Peterson, R. G., and L. Stramma (1991), Upper-level circulation in the South Atlantic Ocean, *Prog. Oceanogr.*, *26*, 1–73.
Pezzi, L. P., and R. B. Souza (2009), Variabilidade de mesoescala e interaçãooceano-atmosfera no AtlânticoSudoeste, in *Tempo e Clima no Brasil*, pp. 385–405, Oficina de Textos, São Paulo, Brasil.
Pezzi, L. P., J. Vialard, K. J. Richards, C. Menkes, and D. Anderson (2004), Influence of ocean-atmosphere coupling on the properties of tropical instability waves, *Geophys. Res. Lett.*, *31*, L16306, doi:10.1029/2004GL019995.
Pezzi, L. P., R. B. Souza, M. S. Dourado, C. A. E. Garcia, M. M. Mata, and M. A. F. Silva Dias (2005), Ocean-atmosphere in-situ observations at the Brazil-Malvinas confluence region, *Geophys. Res. Lett.*, *32*, L22603, doi:10.1029/2005GL023866.
Pezzi, L. P., R. B. de Souza, O. Acevedo, I. Wainer, M. M. Mata, C. A. E. Garcia, and R. de Camargo (2009), Multiyear measurements of the oceanic and atmospheric boundary layers at the Brazil-Malvinas confluence region, *J. Geophys. Res.*, *114*, D19103, doi:10.1029/2008JD011379.
Piola, A. R. and A. L. Rivas (1997), Corrientes en La Plataforma continental, in El Mar Argentino y sus recursos pesqueros. Tomo 1: Antecedentes históricos de lasexplotacionesenel mar y las características ambientales, edited by E. E. Boschi, pp.119–132, Instituto Nacional de Investigación y Desarrollo Pesquero (INIDEP), Mar del Plata.
Piola, A. R., E. J. Campos, O. O. Möller, M. Charo, and C. Martinez (2000), Subtropical shelf front off eastern South America, *J. Geophys. Res.*, *105*(C3), 6565–6578.
Piola, A. R., O. O. Möller, R. A. Guerrero, and E. J. D. Campos (2008), Variability of the Subtropical Shelf front off eastern South America: Winter 2003 and summer 2004, *Cont. Shelf Res.*, *28*, 1639–1648, doi:10.1016/j.csr.2008.03.013.
Piva, E., M. C. D. L. Moscati, and M. A. Gan (2008), Role of surface latent and sensible heat fluxes associated to a South America East Coast cyclogenesis case, *Rev. Bras. Meteorol.*, *23*(4), 450–476.
Piva, E., M. A. Gan, and M. C. L. Moscati (2011), The role of latent and sensible heat fluxes in an explosive cyclogenesis over South America, *J. Meteorol. Soc. Jpn.*, *89*(6), 1–27, doi:10.2151/jmsj.2011-604.
Rouault, M., C. J. C. Reason, J. R. E. Lutjeharms, and A. C. M. Beljaars (2003), Underestimation of latent and sensible heat fluxes above the Agulhas current in NCEP and ECMWF analyses. *J. Clim.*, *16*, 776–782.
Saha, S., et al. (2010), The NCEP climate forecast system reanalysis, *Bull. Am. Meteorol. Soc.*, *91*, 1015–1057.
Saha, S., et al. (2014), The NCEP Climate Forecast System Version 2. *J. Clim.*, *27*, 2185–2208, doi:10.1175/JCLI-D-12-00823.1.
Seluchi, M., and A. C. Saulo (1998), Possible mechanisms yielding an explosive coastal cyclogenesis over South America: Experiments using a limited area model, *Aust. Meteorol. Mag.*, *47*(4), 309–320.
Seo, H., A. J. Miller, and J. O. Roads (2007), The Scripps Coupled Ocean-Atmosphere Regional (SCOAR) model, with applications in the eastern Pacific sector, *J. Clim.*, *20*, 381–402, doi:10.1175/JCLI4016.
Silva Dias, P. L., M. A. F. da Silva Dias, M. Seluchi, and F. de Assis Diniz (2004), O ciclone Catarina: Análise preliminar da estrutura, dinâmica e previsibilidade, in *Congresso Brasileiro de Meteorologia*, vol. XIII, Anais eletrônicos. . . Soc. Bras. de Meteorol.-SBMET, Fortaleza. [Available at Disponível em: <http://www.cbmet.com/=.]
Small, R. J., S. P. de Szoeke, S. P. Xie, L. O'Neill, H. Seo, Q. Song, P. Cornillon, M. Spall, and S. Minobe (2008), Air-sea interaction over ocean fronts and eddies, *Dyn. Atmos. Oceans*, *45*, 274–319, doi:10.1016/j.dynatmoce.2008.01.001.
Smith, M. J., D. T. Ho, C. S. Law, J. McGregor, S. Popinet, and P. Schlosser (2010) Uncertainties in gas exchange parameterization during the SAGE dual-tracer experiment, *Deep Sea Res., Part II*, *58*, 869–881, doi:10.1016/j.dsr2.2010.10.025.
Spall, M. A. (2007), Midlatitude wind stress-sea surface temperature coupling in the vicinity of oceanic fronts, *J. Clim.*, *20*(15), 3785–3801.
Soares, H. C., D. F. M. Gherardi, L. P. Pezzi, M. T. Kayano, and E. T. Paes (2014), Patterns of interannual climate variability in Large Marine Ecosystems. *J. Marine Sys. 134*, 57–68, doi:10.1016/j.jmarsys. 2014.03.004.
Souza, R. B., and I. S. Robinson (2004), Lagrangian and satellite observations of the Brazilian Coastal Current, *Cont. Shelf Res.*, *24*, 241–262.
Stark, J. D., C. J. Donlon, M. J. Martin, and M. E. McCulloch (2007), OSTIA: An operational, high resolution, real time, global sea surface temperature analysis system, in *Oceans 07 IEEE Aberdeen, Conference Proceedings on Marine Challenges: Coastline to Deep Sea*, IEEE, Aberdeen, Scotland.
Stull, R. B. (1998), *An Introduction to Boundary Layer Meteorology*, 666 pp., Kluwer Acad., Dordrecht, Netherlands.
Sunye, P. S., and J. Servain (1998), Effects of seasonal variations in meteorology and oceanography on the Brazilian sardine fishery, *Fish. Oceanogr.*, *7*(2), 89–100.
Tanimoto, Y., T. Kanenari, H. Tokinaga, and S. P.Xie (2011), Sea level pressure Minimum along the Kuroshio and its extension, *J. Clim.*, *24*(16), 4419–4434.
Tokinaga, H., Y. Tanimoto, and S.-P. Xie (2005), SST-induced surface wind variations over the Brazil-Malvinas Confluence: Satellite and in situ observations, *J. Clim.*, *18*, 3470–3482.
Vianna, M. L., V. V. Menezes, A. B. Pezza, and I. Simmonds (2010), Interactions between Hurricane Catarina (2004) and warm core rings in the South Atlantic Ocean, *J. Geophys. Res.*, *115*, C07002, doi:10.1029/2009JC005974.
Wallace, J. M., T. P. Mitchell, and C. J. Deser (1989), The influence of sea surface temperature on surface wind in the eastern equatorial Pacific: Weekly to monthly variability, *J. Clim.*, *2*, 1492–1499, doi:10.1175/1520-0442(1989)002 <1492:TIOSST>2.0.CO;2.
Xie, S. P. (2004), Satellite observations of cool ocean-atmosphere interaction, *Bull. Am. Meteorol. Soc.*, *85*, 195–208, doi:10.1175(BAMS-82-2-195).
Xu, H., H. Tokinaga, and S.-P. Xie (2010), Atmospheric effects of the Kuroshio large meander during 2004-05, *J. Clim.*, *23*, 4704–4714.
Xu, H., M. Xu, S.-P. Xie, and Y. Wang (2011), Deep atmospheric response to the spring Kuroshio over the East China Sea, *J. Clim.*, *24*, 4959–4972.
Yu, L., Z. Zhang, S. Zhong, M. Zhou, Z. Gao, H. Wu, and B. Sun (2011), An inter-comparison of six latent and sensible heat flux products over the southern ocean, *Polar Res.*, *30*, suppl.1, 10167, doi:10.3402/polar.v30i0.10167.
Zavialov, P., O. Möller, and E. Campos (2002), First direct measurements of currents on the continental shelf of southern Brazil, *Cont. Shelf Res.*, *22*(14), 1975–1986.